SARS-CoV-2 nsp16 is regulated by host E3 ubiquitin ligases, UBR5 and MARCHF7

Li Tian[1#], Zongzheng Zhao[2#], Wenying Gao[1], Zirui Liu [2], Xiao Li[2*], Wenyan Zhang[1*] and Zhaolong Li[1*]

[1]Department of Infectious Diseases, Infectious Diseases and Pathogen Biology Center, Institute of Virology and AIDS Research, Key Laboratory of Organ Regeneration and Transplantation of The Ministry of Education, The First Hospital of Jilin University, Changchun 130000, Jilin, China

[2]Research Unit of Key Technologies for Prevention and Control of Virus Zoonoses, Chinese Academy of Medical Sciences, Changchun Veterinary Research Institute, Chinese Academy of Agricultural Sciences, Changchun 130000, Jilin, China

[#]These authors contributed equally to this article.

*Correspondence:

Wenyan Zhang (zhangwenyan@jlu.edu.cn), Xiao Li (skylee6226@163.com), and Zhaolong Li (lizhaolong@jlu.edu.cn)

Competing Interests: The authors declare no conflicts of interest.

Abstract

Severe acute respiratory syndrome coronavirus 2 (SARS-CoV-2), the causative agent of coronavirus disease 2019 (COVID-19), remains a global public health threat with considerable economic consequences. The non-structural protein 16 (nsp16), in complex with nsp10, facilitates the final viral mRNA capping step through its 2′-O-methylase activity, helping the virus to evade host immunity and prevent mRNA degradation. However, nsp16 regulation by host factors remains poorly understood. While various E3 ubiquitin ligases interact with SARS-CoV-2 proteins, their roles in targeting nsp16 for degradation are unclear. In this study, we demonstrate that nsp16 undergoes ubiquitination and proteasomal degradation mediated by the host E3 ligases UBR5 and MARCHF7. UBR5 induces K48-linked ubiquitination, whereas MARCHF7 promotes K27-linked ubiquitination, independently suppressing SARS-CoV-2 replication in vitro and in vivo. Notably, UBR5 and MARCHF7 also degrade nsp16 variants from different viral strains, exhibiting broad-spectrum antiviral activity. Our findings reveal novel antiviral mechanisms of the ubiquitin-proteasome system (UPS) and highlight their potential therapeutic targets against COVID-19.

Key words: SARS-CoV-2, nsp16, ubiquitination, UBR5, MARCHF7, proteasomal degradation

Introduction

Severe acute respiratory syndrome coronavirus 2 (SARS-CoV-2) remains a global public health threat, with over 641 million coronavirus disease 2019 (COVID-19) cases and 6.6 million deaths as of December 2022 (Carabelli et al., 2023; Markov et al., 2023). The virus encodes four structural proteins, 16 non-structural proteins (nsps) involved in replication and transcription, and several accessory proteins (ORFs) linked to immune evasion (V'kovski et al., 2021; Wang et al., 2020). Many viruses, including Ebola (Valle et al., 2021), dengue (Jung et al., 2018), and reovirus (Furuichi et al., 1975), encode 2'-O methyltransferases (2'-O-MTases) that mimic the host 5' cap structure to evade innate immune recognition (Daffis et al., 2010; Züst et al., 2011). Similarly, SARS-CoV-2 nsp16, in complex with nsp10, functions as a 2′-O-MTase, modifying capped viral RNA from 'cap-0' to 'cap-1' (Benoni et al., 2021; Park et al., 2022). This modification protects the virus from host antiviral defences, such as MDA5 recognition and IFIT1 restriction (Bergant et al., 2022; Russ et al., 2022). Beyond immune evasion, nsp16 disrupts global host mRNA splicing, reducing cellular protein and mRNA levels (Banerjee et al., 2020). Nsp16 also enhances SARS-CoV-2 entry by upregulating TMPRSS2 expression (Han et al., 2023), underscoring its role as a virulence factor. Notably, nsp16-deficient strains exhibit low pathogenicity and elicit robust immune responses, suggesting their potential as live-attenuated vaccines (Ye et al., 2022). Given the critical functions of nsp16, inhibitors targeting nsp16 or the nsp16–nsp10 complex have been developed (Klima et al., 2022; Nguyen et al., 2022). Therefore, understanding host factors that regulate nsp16 is essential for identifying new therapeutic strategies.

The ubiquitin-proteasome system (UPS) is a key pathway for targeted protein degradation, often described as 'the molecular kiss of death' (Dongdem & Wezena, 2021; Park et al., 2020). Substrate ubiquitination involves a cascade of three enzymes: E1 activating enzyme, E2 conjugating enzyme, and E3 ubiquitin ligase (Zheng & Shabek, 2017). Some E3 ubiquitin ligases function as monomers, whereas others assemble into multi-subunit complexes. Regardless of their structure, all E3 ligases play a crucial role in

substrate recognition, dictating UPS specificity. In certain complexes, an additional protein may function as a substrate receptor, mediating substrate-specific recognition (Iconomou & Saunders, 2016; Yang et al., 2021; Li et al., 2021; Wang et al., 2022). Over 600 E3 ligases encoded in the human genome regulate diverse cellular processes in response to various signals (Dongdem & Wezena, 2021; Garcia-Barcena et al., 2020). Dysregulation of their activity is linked to multiple diseases, making them attractive therapeutic targets (Humphreys et al., 2021). Based on conserved domains and ubiquitin (Ub) transfer mechanisms, E3 ligases are categorised into three classes: Really Interesting New Gene (RING), homologous to the E6AP carboxyl terminus (HECT), and RING-between-RING (RBR) ligases (Garcia-Barcena et al., 2020; Morreale & Walden, 2016). RING E3s transfer Ub directly from the E2-Ub complex to substrates (Deshaies & Joazeiro, 2009), whereas HECT-type E3s first attach Ub to their own catalytic cysteine before transferring it (Huibregtse et al., 1995). These distinct mechanisms highlight the complexity and versatility of E3 ligase function in cellular regulation (Walden & Rittinger, 2018; Garcia-Barcena et al., 2020).

To investigate the relationship between SARS-CoV-2 and host factors, we focused on UPS proteins that interact with nsp16. In this study, we demonstrate for the first time that nsp16 undergoes ubiquitination and proteasomal degradation. Notably, two E3 ligases from distinct families—RING-type MARCHF7 and HECT-type UBR5—independently target nsp16 for degradation, disrupting its function and exhibiting strong antiviral activity against SARS-CoV-2. Our findings reveal novel therapeutic targets for combating SARS-CoV-2 and treating COVID-19.

Results

SARS-CoV-2 nsp16 is degraded via the ubiquitin-proteasome pathway

Ubiquitination plays a crucial role in SARS-CoV-2 infection and pathogenesis (Gao et al., 2022; Guo et al., 2021; Li et al., 2023; Zhang et al., 2021; Zhang et al., 2024; Zhang et al., 2023). To determine whether SARS-CoV-2 non-structural proteins (nsps) are UPS-regulated, we examined the effect of the proteasome inhibitor, MG132, on nsps expression. MG132 treatment significantly increased the nsp8, nsp11, and nsp16 abundance in HEK293T cells (Fig. 1A), suggesting UPS-mediated degradation. Nsp8 undergoes TRIM22-mediated ubiquitination and proteasomal degradation (Fan et al., 2024). In this study, we focused on nsp16 for further investigation. To confirm UPS-mediated nsp16 degradation, we tested additional proteasome inhibitors, Bortezomib and Carfilzomib, both of which enhanced nsp16 stability. In contrast, lysosomal inhibitors (Bafilomycin A1 and NH_4Cl) and the autophagy-lysosomal inhibitor, Vinblastine, had no such effect (Fig. 1B). To further assess the role of the UPS in regulating nsp16 stability, we treated nsp16-expressing cells with cycloheximide, a protein synthesis inhibitor, and measured the half-life of nsp16. MG132 treatment significantly prolonged nsp16 stability, extending its half-life from 2 h to 15 h (Fig. 1C and 1D).

To identify nsp16-interacting proteins, we performed co-immunoprecipitation (Co-IP) followed by mass spectrometry (MS) analysis, comparing nsp16-expressing cells with and without MG132 treatment (Fig. 1E). Kyoto Encyclopedia of Genes and Genomes (KEGG) pathway and Gene Ontology (GO) analyses (Figure 1—figure supplement 1A) revealed that inhibiting nsp16 degradation increased its interacting proteins, including 43 associated with viral processes, 22 involved in mRNA stability regulation, and five linked to cellular antiviral defence. Additionally, interactions related to mRNA splicing and RNA methylation were identified (Banerjee et al., 2020), consistent with the function of nsp16 as a 2′-O-MTase. Furthermore, SARS-CoV-2 exploits nsp16 to disrupt host mRNA splicing, which promotes infection (Park et al., 2022; Russ et al., 2022; Züst et al., 2011), further validating our MS data.

As expected, several nsp16-binding proteins were associated with ubiquitination and degradation pathways (Figure 1–figure supplement 1B). We identified four deubiquitinases (DUBs), the E2 ligase UBE2D3, and 14 proteasomal enzymes. Among them, six E3 ligases—UBR5, MARCHF7, HECTD1, TRIM32, MYCBP2, and TRIM21—were selected for further investigation.

E3 ligases, UBR5 and MARCHF7, independently mediate nsp16 degradation

To identify the E3 ligases responsible for nsp16 degradation, we designed small interfering RNAs (siRNAs) targeting six candidate E3 ligases and assessed their effects on nsp16 abundance. UBR5 and MARCHF7 knockdown significantly stabilised nsp16 protein levels (Fig. 2A). To further investigate their roles in nsp16 degradation, we generated stable cell lines with UBR5 or MARCHF7 knockdowns and confirmed silencing efficiency (Fig. 2B). To determine whether UBR5 and MARCHF7 function cooperatively, we performed dual knockdowns. Silencing UBR5 in MARCHF7-knockdown cells, and vice versa, further enhanced nsp16 stability, indicating that these ligases act independently (Fig. 2C). Overexpression studies further supported their independent roles—MARCHF7 overexpression induced nsp16 degradation even in MARCHF7-knockdown and MARCHF7/UBR5 double-knockdown cells. Similarly, UBR5 overexpression promoted nsp16 degradation despite MARCHF7 knockdown. Silencing efficiencies were validated across all experiments (Figure 2—figure supplement 1A and 1B). Notably, wild-type MARCHF7 and UBR5, but not their mutants lacking functional RING (1-542 aa) or HECT domains, respectively, effectively degraded nsp16 in knockdown cells (Fig. 2D and 2E). These findings confirm that UBR5 and MARCHF7 independently mediate nsp16 ubiquitination via their HECT and RING domains, targeting it for proteasomal degradation.

UBR5 and MARCHF7 mediate distinct Ub linkages on nsp16

We first confirmed nsp16 ubiquitination both with and without exogenous ubiquitin (Ub) expression (Fig. 3A-B). To investigate the role of E3 ligases in this process, we examined the impact of UBR5 and MARCHF7 knockdown on nsp16 ubiquitination. Silencing either ligase reduced nsp16 ubiquitination compared to the negative control, indicating their

involvement in this modification (Fig. 3C). Ub contains seven lysine residues (K6, K11, K27, K29, K33, K48, and K63), which form polyubiquitin chains with distinct functions that determine the fate of the attached protein (Grice & Nathan, 2016). To identify the specific polyubiquitin chain types formed on nsp16 by UBR5 and MARCHF7, we used a series of Ub mutants, each retaining only a single lysine residue. Except for K33, all single-lysine Ub mutants supported nsp16 ubiquitination to varying degrees, suggesting a complex ubiquitin architecture potentially regulated by multiple E3 ligases or E2-E3 pairs (Fig. 3D). Further analysis of lysine-specific linkages revealed that MARCHF7 primarily mediates K27-linked ubiquitination of nsp16, whereas UBR5 facilitates K48-linked ubiquitination (Fig. 3E and 3F). These findings establish that UBR5 and MARCHF7 independently regulate nsp16 degradation through distinct ubiquitin linkages.

UBR5 and MARCHF7 directly interact and colocalise with nsp16 in the endoplasmic reticulum (ER)

MS analysis suggested interactions between nsp16 and both UBR5 and MARCHF7. Co-IP experiments confirmed that Myc-tagged MARCHF7 and endogenous UBR5 bind to nsp16 (Figure 4—figure supplement 1A and 1B). To assess whether these interactions are direct, we performed fluorescence resonance energy transfer (FRET) assays. When nsp16-YFP was bleached, the fluorescence intensity of CFP-UBR5 and CFP-MARCHF7 increased, confirming direct interactions (Figure 4 — figure supplement 1C). ImageJ software was used to quantify relative fluorescence intensities (Figure 4 — figure supplement 1D). To determine whether UBR5 and MARCHF7 depend on each other for nsp16 binding, we examined the effect of MARCHF7 knockdown on UBR5-nsp16 interactions, and vice versa, using Co-IP. The interactions remained unchanged, indicating that UBR5 and MARCHF7 independently bind to nsp16 (Fig. 4A and 4B). Nsp16 localises to both the nucleus and cytoplasm (Zhang et al., 2020). UBR5 (containing two nuclear localization signals) and MARCHF7 are also present in both compartments (Muñoz-Escobar et al., 2015; Shearer et al., 2018) (Nathan et al., 2008). Immunofluorescence staining revealed that UBR5 and MARCHF7 colocalised with nsp16 predominantly in the

180 cytoplasm, with some nuclear colocalization observed in HeLa cells (Figure 4—figure
181 supplement 1E). Similar results were obtained in nsp16-transfected HEK293T cells using
182 antibodies against endogenous UBR5 and MARCHF7 (Figure 4—figure supplement 1F).

183 To pinpoint the specific cellular compartment where these interactions occur, we co-
184 transfected UBR5-CFP or MARCHF7-CFP with nsp16-YFP and performed
185 immunostaining using organelle-specific markers: COX5A (mitochondria), PDI (ER), and
186 GM130 (Golgi apparatus). Notably, UBR5 and MARCHF7 both interacted with nsp16 and
187 colocalised with PDI, but not with COX5A or GM130 (Fig. 4C and 4D), indicating that both
188 E3 ligases interact with nsp16 primarily in the ER.

189 **Functional domains of UBR5 and MARCHF7 are required for nsp16 interaction and**
190 **ubiquitination**

191 UBR5 is a four-domain E3 ligase containing two nuclear localization signals. Its
192 domains include UBA, UBR, PABC, and HECT (Muñoz-Escobar et al., 2015) (Figure 4—
193 figure supplement 2A). Notably, the HECT domain is critical for its E3 ligase activity, as
194 UBR5 must first conjugate to Ub before transferring it to substrates (Kim et al., 2021). To
195 determine which UBR5 domain mediates nsp16 ubiquitination, we used UBR5 mutants
196 with individual domain inactivations. Only the HECT domain mutant failed to degrade
197 nsp16 (Figure 4—figure supplement 2B), consistent with previous studies (Zhou et al.,
198 2022). This mutant also lost the ability to ubiquitinate nsp16, confirming the essential role
199 of the HECT domain in this process (Figure 4—figure supplement 2C).

200 To identify the MARCHF7 region responsible for nsp16 degradation, we generated a
201 series of truncation mutants as described previously (Figure 4—figure supplement 2D)
202 (Zhao et al., 2018) (Nathan et al., 2008). All mutants lost the ability to degrade nsp16
203 (Figure 4—figure supplement 2E). Further analysis revealed that only the mutant
204 containing the intact N-terminal region (aa 1–542) strongly bound to nsp16, while those
205 retaining the active RING domain region (aa 543–616) did not. Consistently, only wild-type
206 MARCHF7 promoted K27-linked ubiquitination of nsp16 (Figure 4—figure supplement 2F).

207 These results indicate that the N-terminal region of MARCHF7 is essential for nsp16
208 binding, whereas its RING domain is required for K27-linked ubiquitination activity.

209 **UBR5 and MARCHF7 suppress SARS-CoV-2 replication by targeting nsp16 for**
210 **degradation**

211 To assess the impact of nsp16 degradation on viral replication, we used a biosafety
212 level 2 system to generate SARS-CoV-2 transmissible virus-like particles capable of
213 infecting Caco2-N^{int} cells (Ju et al., 2021). Knockdown of either UBR5 or MARCHF7
214 significantly increased SARS-CoV-2 replication, with simultaneous knockdown further
215 enhancing viral replication (Figure 5—figure supplement 1A and 1B).

216 To investigate nsp16 modifications following infection, we infected HEK293T-ACE2
217 cells with the Wuhan strain for 48 h. Co-IP using an anti-nsp16 antibody confirmed its
218 interaction with endogenous MARCHF7 and UBR5, along with ubiquitination (Fig. 5A). In
219 a biosafety level 3 facility, we further validated the antiviral roles of UBR5 and MARCHF7
220 using the Wuhan (MOI 0.01) and Omicron strains (MOI 0.001). Knockdown of either E3
221 ligase in Caco2 cells significantly increased intracellular and secreted viral mRNA levels
222 (M and E genes) for both strains. Viral titres in the supernatants also increased, with UBR5
223 knockdown causing over a 1-log rise for the Wuhan strain and even greater effects for
224 Omicron (Fig. 5C–E and 5F–H for the Wuhan and Omicron strains, respectively).
225 Immunoblotting confirmed increased intracellular and secreted N protein levels upon UBR5
226 or MARCHF7 knockdown (Fig. 5I), with knockdown efficiencies verified (Fig. 5B). Due to
227 low transfection efficiency in Caco2 cells, we overexpressed UBR5-Myc or MARCH7-Myc
228 in HEK293T-ACE2 cells. Overexpression significantly reduced viral mRNA (M and E genes)
229 and N protein levels in both strains, accompanied by a 0.5-log decrease in viral titres.
230 However, co-transfection with increasing nsp16 levels counteracted these inhibitory effects
231 (Fig. 6A–H and Figure 6—figure supplement 1A–H). To confirm the role of UBR5 and
232 MARCHF7 enzymatic activity, we overexpressed catalytically inactive mutants (UBR5-Δ
233 HECT or MARCHF7-aa 1-542) alongside nsp16. These mutants failed to suppress viral
234 replication. Additionally, gradual increases in nsp16 expression did not further enhance

235 viral replication, with only a slight increase in M mRNA, while E and N protein levels
236 remained unchanged (Figure 6—figure supplement 2A–H). These findings demonstrate
237 that UBR5 and MARCHF7 exert antiviral effects by ubiquitinating and degrading nsp16,
238 thereby significantly inhibiting SARS-CoV-2 replication.

239 **UBR5 and MARCHF7 mediate nsp16 variant degradation**

240 With the continuous emergence of SARS-CoV-2 variants, broad-spectrum antiviral
241 strategies have become essential. To assess whether UBR5 and MARCHF7 mediate
242 various nsp16 variants, we analysed nsp16 amino acid sequences from the National
243 Center for Biotechnology Information (NCBI) (Figure 6—figure supplement 3A). Most
244 variants had one or two mutations, except for XBB.1.9.1, XBB.1.5, and XBB.1.16, which
245 contained more mutations, suggesting a conserved sequence. We used mutagenesis to
246 synthesise nsp16 sequences for these three variants, along with several single-site
247 mutants from other variants. Treatment with MG132 restored nsp16 protein levels for all
248 variants (Figure 6—figure supplement 3B), confirming UPS-mediated degradation.
249 Furthermore, UBR5 or MARCHF7 knockdown stabilised nsp16 proteins from these
250 variants, though to varying degrees (Figure 6—figure supplement 3C). These results
251 suggest that UBR5 and MARCHF7 contribute to broad-spectrum antiviral activity by
252 targeting nsp16 from diverse SARS-CoV-2 variants for degradation.

253 **SARS-CoV-2 infection reduces UBR5 and MARCHF7 expression**

254 To investigate the impact of SARS-CoV-2 infection on UBR5 and MARCHF7
255 expression, we analysed their mRNA and protein levels following infection with the Wuhan
256 and Omicron strains at varying MOIs using RT-qPCR and immunoblotting. MARCHF7
257 expression decreased consistently with increasing viral titres, whereas UBR5 levels initially
258 rose at low titres before declining as infection progressed (Figure 6—figure supplement
259 4A-4C). This transient UBR5 upregulation may be linked to its role in interferon-γ-mediated
260 pathways, as previously reported (Wu et al., 2022). To confirm these findings in vivo, we
261 examined UBR5 and MARCHF7 mRNA levels in peripheral blood mononuclear cells from
262 SARS-CoV-2-infected patients with varying disease severity. UBR5 expression negatively

correlated with disease progression, whereas MARCHF7 levels showed no significant correlation (Figure 6—figure supplement 4D). These results suggest that SARS-CoV-2 may actively suppress host antiviral defences by downregulating UBR5 and MARCHF7 expression.

UBR5 and MARCHF7 protect mice from SARS-CoV-2 challenge

Since no specific activators or inhibitors for E3 ligases are available, we used a transient overexpression method using high-pressure tail vein injection of plasmids in mice (Bonamassa et al., 2011). To evaluate their antiviral effects in vivo, mice were injected with plasmids encoding UBR5 or MARCHF7, followed by SARS-CoV-2 challenge (Fig. 7A). E3 ligase overexpression significantly reduced viral E gene copy numbers in the lungs and markedly decreased viral titres (Fig. 7C-D). Additionally, treated mice experienced less weight loss compared to controls (Fig. 7E). Histopathological analysis at 5 days post-infection showed that lungs from UBR5- or MARCHF7-treated mice exhibited reduced alveolar contraction and pulmonary oedema compared to the severe lesions observed in control mice (Fig. 7F). Immunoblotting further confirmed lower N protein abundance in treated mice (Fig. 7G). These results suggest that UBR5 and MARCHF7 overexpression suppresses SARS-CoV-2 virulence in vivo by promoting nsp16 degradation.

SARS-CoV-2 infection can induce a severe cytokine storm, contributing to high mortality rates (Song et al., 2020) (Hojyo et al., 2020). To assess the impact of UBR5 and MARCHF7 on inflammatory responses, we measured key cytokine levels—including interleukin-6 (IL-6), interleukin-1 receptor antagonist (IL-1RA), and interleukin-1β (IL-1β)—in the spleens of infected mice (Makaremi et al., 2022) (Hu et al., 2021). Consistent with their antiviral activity, UBR5 and MARCHF7 treatment significantly reduced the production of these inflammatory cytokines (Fig. 7H).

Discussion

SARS-CoV-2 nsp16 functions as a 2′-O-methyltransferase (2′-O-MTase), catalysing penultimate nucleotide methylation of the viral RNA cap. This modification allows SARS-CoV-2 to mimic host mRNA, evading immune detection and response (Lin et al., 2020) (Balieiro et al., 2022; Russ et al., 2022). High-resolution structures of nsp16 and nsp16-nsp10 heterodimers have been characterised (Rosas-Lemus et al., 2020) (Klima et al., 2022; Lugari et al., 2010), providing a foundation for antiviral drug development targeting these complexes (Balieiro et al., 2022; Melo-Filho et al., 2022). However, host factors that interact with and regulate nsp16 remain largely unknown.

Previous studies, including work from our group, have highlighted the role of the UPS in modulating SARS-CoV-2 infection (Xu et al., 2022). Several host E3 ligases—such as RNF5, Cullin4-DDB1-PRPF19, ZNF598, and TRIM7 — ubiquitinate and degrade key SARS-CoV-2 proteins, thereby suppressing viral replication (Li et al., 2023; Liang et al., 2022; Maimaitiyiming et al., 2022; Zhang et al., 2024). In contrast, SARS-CoV-2 uses deubiquitinases (DUBs) to counteract these defences and enhance viral replication (Chen et al., 2024; Gao et al., 2024; Gao et al., 2022; Guo et al., 2021). In this study, we identify nsp16 as a short-lived protein with a half-life of only 2 – 3 h, which is targeted for ubiquitination and degradation via the UPS. Using MS and bioinformatics screening, we identified two E3 ligases, UBR5 and MARCHF7, that directly interact with nsp16 and mediate nsp16 ubiquitination and degradation.

UBR5, a member of the UBR box protein family, contains a HECT domain essential for its E3 ligase activity (Kim et al., 2021). UBR5 regulates tumour growth, metastasis (Xiang et al., 2022) (Qiao et al., 2020), and viral infections. For instance, UBR5 targets the ORF4b protein of Middle East respiratory syndrome coronavirus (MERS-CoV) for degradation, reducing its ability to counteract the host immune response (Zhou et al., 2022). Conversely, UBR5 supports Zika virus replication by assisting TER94/VCP in degrading the capsid protein, allowing viral genome release into the cytoplasm (Gestuveo et al.).

316 MARCHF7, a RING E3 ligase, plays a role in T cell proliferation, neuronal development,
317 inflammasome regulation, and tumour progression (Zheng, 2021) (Zhang et al., 2016) (Cai
318 et al., 2022) (Zhao et al., 2018). However, its involvement in viral infections remains largely
319 unexplored, with one study identifying it as a host protein interacting with the 2C protein of
320 foot-and-mouth disease virus (Mahajan et al., 2021).

321 Our findings demonstrate that UBR5 and MARCHF7 independently interact with
322 nsp16 and facilitate its degradation, primarily on the cytoplasmic ER. Our findings highlight
323 the ongoing evolutionary battle between viruses, which evolve strategies to evade host
324 defences, and hosts, which deploy multiple mechanisms to counteract viral infections. One
325 such strategy is the use of multiple E3 ligases targeting the same viral protein for
326 degradation. Functional analyses revealed that knocking down UBR5 or MARCHF7
327 enhanced SARS-CoV-2 replication, whereas their overexpression impaired it. Moreover,
328 when their enzymatic activity was inactivated, the antiviral effect was abolished, confirming
329 that their E3 ligase activity is essential for viral suppression. Notably, nsp16 overexpression
330 alone did not increase viral levels in the absence of functional UBR5 or MARCHF7. This
331 underscores the critical antiviral role of UBR5 and MARCHF7 in restricting SARS-CoV-2
332 by promoting nsp16 degradation.

333 Due to the presence of 18 lysine residues in nsp16, identifying specific ubiquitination
334 sites was challenging. Using structural data (Decroly et al., 2011), we constructed truncated
335 nsp16 mutants to assess their degradation profiles. Our results showed that nsp16 mutants
336 degradation occurred to varying degrees (Appendix-figure S2A-B), suggesting that multiple
337 lysine residues serve as recognition sites for E3 ligases. Furthermore, MG132 recovery
338 experiments provided valuable insights. The △2-17 mutant, which lacks this segment,
339 exhibited more than a two-fold increase in nsp16 expression, whereas the △204-212
340 mutant showed significantly reduced recovery after MG132 treatment compared to the
341 wild-type. These observations offer important clues for further investigation into the
342 interaction regions between nsp16 and MARCHF7 or UBR5, as well as potential
343 ubiquitination sites. MS analysis identified K76 as a ubiquitination site (Appendix-figure

344 S2C). However, the nsp16 K76R mutant still underwent degradation, though its
345 ubiquitination level was reduced compared to that of the wild-type, indicating that K76 is
346 one of several ubiquitination sites (Appendix-figure S2D-E). This suggests that nsp16 may
347 undergo ubiquitination at multiple sites or through non-canonical pathways at non-lysine
348 residues (McClellan et al., 2019). Beyond UBR5 and MARCHF7, other E3 ligases may also
349 contribute to nsp16 regulation, warranting further investigation into additional host factors
350 involved in SARS-CoV-2 restriction.

351 Currently, no specific activators or inhibitors exist for UBR5 or MARCHF7. To assess
352 their antiviral effects in vivo, we used high-pressure tail vein injection, a gene delivery
353 method primarily targeting the liver (Kamimura et al., 2014) but also effective for lung
354 tissues (Bonamassa et al., 2011). Gene expression was successfully detected in the lungs,
355 and while this method induced mild immune activation, its effect was minimal compared to
356 other techniques (Suda et al., 2023). Notably, mice and non-human primates exhibit
357 greater resistance to innate immune activation than humans (Raper et al., 2003),
358 suggesting that immune activation had little influence on our results. However, translating
359 these findings into therapeutic applications remains challenging. For instance, human trials
360 using naked DNA injections (e.g., OTC cDNA) have shown variable immune responses,
361 with one case of fatal immune activation reported (Raper et al., 2003). This underscores
362 the variability of human immune responses and the challenges in translating findings from
363 animal models to clinical applications. Such variability may also explain the inconsistent
364 trends in MARCHF7 mRNA levels observed in peripheral blood samples from patients with
365 different disease severities. Additionally, the small sample size in our study may have
366 contributed to this observation.

367 In conclusion, in this study, we identified the host E3 ligases UBR5 and MARCHF7 as
368 key regulators of SARS-CoV-2 nsp16, facilitating its ubiquitination and degradation. We
369 observed a negative correlation between their expression levels and infection severity,
370 highlighting their antiviral function. Moreover, both ligases effectively suppressed SARS-
371 CoV-2 replication. These findings provide a foundation for developing UPS-targeted
372 therapeutic strategies for COVID-19 treatment.

Materials and Methods

Reagents and antibodies

The drugs used in this study were as follows: MG132 (catalog no. S2619), Bafilomycin A1 (catalog no. S1413), Bortezomib (catalog no. S1013), Carfilzomib (catalog no. S2853) and Vinblastine (catalog no. S4504) were purchased from Selleck (Houston, TX, USA). Cycloheximide (catalog no. 66-81-9) was purchased from Sigma (Saint Louis, MO, USA). The antibodies used for immunoblotting analysis (IB) were as follows: anti-UBR5 mAb (Proteintech, Rosemont, IL, USA, catalog no. 66937-1-Ig), anti-MARCHF7 mAb (Santa Cruz Biotechnology, Dallas, TX , USA, catalog no. sc-166945), SARS-CoV-2 2'-O-ribose Methytransferase Antibody (nsp16) (Cell signaling, Danvers, Massachusetts, USA, catalog no. #70811), anti-Flag mAb (Sigma, catalog no. F1804), anti-tubulin mAb (Abcam, Cambridge, Cambridgeshire, UK, catalog no. ab11323), anti-hemagglutinin (anti-HA) pAb (Invitrogen, catalog no. 71-5500), anti-Myc pAb (Proteintech, Rosemont, IL, USA, catalog no. 16286-1-AP), and anti-GFP mAb (Abcam, catalog no. ab1218). Primary antibody: anti-COX5A pAb (Sangon Biotec, Shanghai, CHN, catalog no. D261450), anti-PDI-mAb (Proteintech, catalog no. 2E6A11) and Human GM130/GOLGA2 Antibody (R&D Systems, Minneapolis, MN, USA, catalog no. AF8199) were used for immunofluorescence, and SARS-CoV-2 nucleocapsid monoclonal antibody (mAb) (GeneTex, Irvine, CA, USA, catalog no. GTX635679) were used for Immunohistochemistry. Fluorescent secondary antibodies: goat anti-Rabbit IgG (H+L) Highly Cross Adsorbed Secondary Antibody, Alexa Fluor Plus 488 (Invitrogen, catalog no. A11001), and goat anti-Rabbit IgG (H+L) Highly Cross Adsorbed Secondary Antibody, Alexa Fluor Plus 568 (catalog no. A-11011) and immunohistochemical secondary antibodies: Streptavidin-Peroxidase Anti-Rabbit IgG kit (catalog no. KIT-9706) were purchased from Invitrogen and maixin (Fuzhou, CHN) respectively.

Cell lines and viruses

The cell lines used in this study include HEK293T cells (catalog no. CRL-11268), Hela cells (catalog no.CRM-CCL-2), Caco2 cells (catalog no. HTB-37). All cell lines were purchased from American Type Culture Collection (ATCC; Manassas, VA, USA) and tested

for mycoplasma. In order to conduct virus related experiments, stable cell lines including Caco2-N^{int} (stably expressing SARS-CoV-2 N gene) and 293T-ACE2 (stably expressing ACE2) were generated in our laboratory. The cells were cultured in a cell incubator containing 5% CO2 at 37°C using Dulbecco's modified Eagle's medium (DMEM; HyClone, Logan, UT, USA) containing 10% heat-inactivated fetal calf serum (FCS, GIBCO BRL, Grand Island, NY, USA), 100 mg/ml penicillin, and 100 ug/ml streptomycin to provide nutrition. We expanded SARS-CoV-2 virus-like-particles (Wuhan-Hu-1, MN908947, Clade:19A) with high replication capacity in Caco2-N^{int} using a biosafety level-2 (BSL-2) cell culture system. The virus infecting the cells include Omicron BA. 1 strain (human/CHN_CVRI-01/2022) and SARS-CoV-2 Wuhan strain (BetaCoV/Beijing/IME-BJ05-2020, GenBank access no. MT291831.1), and mouse adapted SARS-CoV-2/C57MA14 variant (GenBank: OL913104.1) used for experiments in mice were provided by Key Laboratory of Jilin Province for Zoonosis Prevention and Control, and all experiments for virus infection were performed in Biosafety level 3 (BSL-3) cell culture system.

Plasmids

Eukaryotic expression plasmids encoding SARS-CoV-2 nsp protein were provided by Professor Wang Peihui (Shandong University). The nsp16-HA expression vector was constructed by adding HA tag at the C-terminus. UBR5 (Gnen ID: 51366) and its mutants (UBR5-ΔHECT, UBR5-ΔPABC, UBR5-ΔUBR) expression plasmids were constructed using purchased plasmids from Addgene (Watertown, MA, USA) as templates with no tag or a MYC tag at the N-terminus. The cDNA of 293T cells was used as a template to construct MARCHF7(Gene ID: 64844) and its truncated mutant with a Myc tag at the C-terminus. All the above expression plasmids were inserted into the VR1012 vector. For immunofluorescence (IF) and Fluorescence Resonance Energy Transfer (FRET) experiments, pCDNA3.1-YFP vector (catalog no. 13033) and pECFP-C1 vector (catalog no. 6076-1) were purchased from Addgene and BD (Biosciences Clontech), and MARCHF7 or UBR5 was constructed on pECFP-C1, and nsp16 was constructed on pCDNA3.1-YFP. Single point mutants of nsp16 of different virus subtypes were obtained

by point mutagenesis. Multi-site combined mutants were synthesized by Sangon Biotec Company. Human ubiquitin protein and its mutants have been previously described. Primers required for PCR were listed in Appendix Table S1.

RNA extraction and real-time quantitative PCR

We used the way of Trizol (Invitrogen, catalog no. 15596018CN) to extract RNA. The RNA was subsequently reverse transcribed using a High-Capacity cDNA Reverse Transcription kit (Applied Biosystems, Carlsbad, CA, USA, catalog no. 4368814). Finally, PrimeScript RT Master Mix (Takara, Shiga, JPN, catalog no. RR036A) and relative real-time primer were used for qPCR on an Mx3005P instrument (Agilent Technologies, Stratagene, La Jolla, CA, USA). Amplification procedure of the target fragment is as follows: predenaturation at 95°C for 2min, denaturation at 95 °C for 30s, annealing at 55 °C for 30s, and extension at 72 °C for 30s, total of 40 cycles. Real-time primer sequences used in this study were shown in appendix table S1.

Immunoblotting analysis (IB)

Cells or supernatant cultured for a certain time were collected, cell precipitates were resuspended with lysis buffer (50 mM Tris–HCl [pH 7.8], 150 mM NaCl, 1.0% NP-40, 5% glycerol and 4 mM EDTA), 4xloading buffer was added (0.08M Tris [pH 6.8], 2.0%SDS, 10% glycerol, 0.1 M dithiothreitol, and 0.2% bromophenol blue), and samples were lysed by heating at 100℃ for 30min. After removal of cell debris by centrifugation, the supernatant was taken to separate proteins of different sizes by SDS-PAGE. The proteins were transferred onto polyvinylidene fluoride (PVDF) membranes, incubated overnight with the indicated primary antibody, and after 1 hour at room temperature with HRP-conjugated secondary antibodies (Jackson Immunoresearch, West Grove, NJ, USA, catalog no. 115-035-062 for anti-mouse and 111-035-045 for anti-rabbit), the proteins were visualized through Ultrasensitive ECL Chemiluminescence Detection Kit (Proteintech, catalog no. B500024).

Stable cell line generation

We purchased the lentiviral vector pLKO.1-puro (catalog no. 8453) from Adggen. ShRNA targeting target genes were designed and synthesized by Sangon Biotech. After

annealing, it was inserted into the vector. Lentivirus was generated by transfection with shRNA (cloned in pLKO.1) or control vector, RRE, VSVG and REV, and the cells were screened with 1/1000 puromycin (3 μg/ml, Sigma, catalog no. P8833) after infection 48 hours. The knockdown efficiency was detected by RT-qPCR or IB. The shRNA target sequences used in this study are shown in appendix table S1.

RNAi

Short interfering RNA (siRNA) used in this study were purchased from RiboBio Co. Ltd. (Guangzhou, CHN). The siRNA sequences for knockdown of MARCHF7 or UBR5 are provided in appendix table S1. The siRNA was transfected into the cells by transfection reagent Lipofectamine 2000 (Invitrogen, catalog no. 11668-019), and the corresponding plasmids were transfected 24 hours later using Lipofectamine 3000 Reagent (Invitrogen, Carlsbad, CA, USA, catalog no. L3000-008). The expression of target genes was detected by RT-qPCR or immunoblotting (IB) analysis 48 hours later.

Immunoprecipitation

After 10 hours of MG132 (10 μM) treatment, the cells were harvested, resuspended in 1ml lysis buffer (50 mM Tris-HCl [pH 7.5], 150 mM NaCl, 0.5% NP-40) containing protease inhibitor (Roche, catalog no. 11697498001), placed on the shaker oscillator for 4 hours to lyse, then centrifuged to remove cell debris, and the supernatant was incubated with the antibody and protein G agarose beads (Roche, Basel, Basel-City, CH, catalog no. 11243233001) at 4°C overnight. Protein G agarose beads was washed 6-8 times with wash buffer (20 mM Tris-HCL [pH 7.5], 100 mM NaCl, 0.1 mM EDTA, and 0.05% Tween 20) at 4°C, centrifuged at 800 g for 1 min. The proteins were eluted by adding loading buffer (0.08 M Tris [pH 6.8], 2.0% SDS, 10% glycerol, 0.1 M dithiothreitol, and 0.2% bromophenol blue), the samples were boiled at 100°C for 10min to elate the proteins. The lysates and immunoprecipitations were detected by IB.

Mass spectrometry (MS)

HEK293T were transfected with SARS-CoV-2-nsp16-Flag for 36 hours, and then harvested after 10 hours of treatment with MG132 or DMSO. Proteins were enriched by

co-immunoprecipitation assay. And the elutions were analyzed by MS. MS analysis was performed by the national center for protein science (Beijing, CHN).

Immunofluorescence

At 48 hours after transfection, the solution was discarded and cells were washed twice with preheated PBS for 5min each, followed by fixation with 4% paraformaldehyde at 37°C for 10min. After three washes with PBS, permeabilized with 0.2% Triton X-100 for 5 min at 37°C, and then immediately followed by blocking with 10% fetal bovine serum at room temperature for 1 hour. The blocked cells were incubated overnight with the indicated primary antibodies. The next day, after three washes with PBS, the cells were incubated with corresponding secondary antibodies for 1 hour at room temperature in the dark. The nuclei were stained with DAPI (49,6-diamidino-2-phenylindole, Sigma, catalog no. 9542) and then stored in 90% glycerol. The fluorescence was detected by a laser scanning confocal microscope (FV 3000, Olympus, Tokyo, Japan).

Viral infectivity assay

The Caco2 cells were transfected with siRNA by Lipofectamine RNAiMAX Reagent (Invitrogen, catalog no. 13778150) to knockdown UBR5 or MARCHF7 and infected with Wuhan strain (MOI=0.01) or Omicron-BA.1 strain (MOI=0.001) at 24 hours after transfection. After two hours of infection, the Caco2 cells were cultured in fresh medium containing 2% fetal bovine serum for 48 hours. The cells and supernatants were collected. Viral levels were characterized by RT-qPCR and IB analysis of viral structural proteins. The overexpression plasmid UBR5-Myc, MARCHF7-Myc and nsp16-Flag was transfected in 293T-ACE2 by Lipofectamine 3000 Reagent and infected with virus 24 hours later.

Mouse lines and infections

BALB/C mice, 6 weeks, were purchased from Charles River Laboratories, Beijing. Mice were cultured in groups according to experimental groups. Our study examined male and female animals, and similar findings are reported for both sexes. To reduce animal suffering, all welfare and experimental procedures were carried out in strict accordance with the Guide for the Care and Use of Laboratory Animals and relevant ethical regulations during the experiment. The mice were randomly divided into 6 groups and injected with 40

μg/500 μl MARCHF7 or UBR5 plasmids via the tail vein at high pressure. Three groups of mice were infected 50ul with SARS-CoV-2 isolates by nasal challenge at a dose of $10^{5.5}$ $TCID_{50}$/mL, three groups were not infected with virus as control, and the empty vector injection group was also used as control.

Immunohistochemical analysis

Three mice in each group, a total of 18 mice, were sacrificed after anesthesia. The lungs of mice were collected and fixed in 4% paraformaldehyde fixative. After 2 days, the lungs were progressively dehydrated through different concentrations of ethanol solution, transparently treated, soaked in xylene, and finally embedded in paraffin. Some thin sections obtained through a microtome for hematoxylin and eosin (H&E) staining. The other fraction was incubated with 3% hydrogen peroxide for 5-10 min at room temperature to eliminate endogenous peroxidase activity. SARS-CoV-2 nucleocapsid monoclonal antibody (mAb) (GeneTex, catalog no. GTX635679) and a Streptavidin-Peroxidase Anti-Rabbit IgG kit (Maixin, Fuzhou, CHN, catalog no. KIT-9706) was used to quantify the viral level in lung tissue.

Statistical analysis

The statistical analyses used in the figures have been described in detail in the figure legends. All data were expressed as mean ± standard deviations (SDs). Statistical comparisons were performed using student's t-test, one-way ANOVA, or repeated measurement ANOVA. The differences were statistically significant as follows: *P < 0.05, **P < 0.01, ***P < 0.001; ns is for no meaning

Ethics statement

Collection of inpatient blood was approved by the Ethics Committee of the First Hospital of Jilin University (21K105-001) in accordance with the guidelines and principles of WMA Declaration of Helsinki and the Department of Health and Human Services Belmont Report. All study participants signed an informed consent form. PBMCS were obtained from 9 COVID-19 patients with mild disease, 6 patients with severe disease, and 5 patients with critical disease (Appendix table S2). All animal experiments were approved by the ethics committee of Research Unit of Key Technologies for Prevention and Control

of Virus Zoonoses, Chinese Academy of Medical Sciences, Changchun Veterinary Research Institute, Chineses Academy of Agricultural Sciences (IACUC of AMMS-11-2020-006).

Acknowledgments

We thank C.Y. Dai for providing critical reagents.

Funding information

This work was supported by funding from the National Natural Science Foundation of China (82341072 and 82272316 to ZWY, 82341062 to LZL), the National Key R&D Program of China (2021YFC2301900 and 2301904, 2023YFC2306603), the Science and Technology Department of Jilin Province (YDZJ202301ZYTS521 and YDZJ202201ZYTS587), the Key Laboratory of Molecular Virology, Jilin Province (20102209), and Bethune Project, Jilin University (2023B03). The funding sources were involved in study design, data collection and interpretation, and the decision to submit the work for publication.

Authors' contributions

L.T.: Conceptualization; Data curation; Formal Analysis; Investigation; Methodology; Writing – original draft. Z.Z.: Methodology; Data curation; Writing – review & editing. Z.L.: Conceptualization; Data curation; Formal Analysis; Investigation; Methodology; Writing – review & editing; Funding acquisition. X.L., Z.L. and W.G.: Methodology; Resources. W.Z.: Conceptualization; Formal Analysis; Funding acquisition; Methodology; Project administration; Resources; Writing – review & editing.

Data availability

The authors declare that [the/all other] data supporting the findings of this study are available within the paper [and its supplementary information files]. The mass spectrometry proteomics data have been deposited to the ProteomeXchange Consortium (http://proteomecentral.proteomexchange.org) via the iProX partner repository with the dataset identified PXD053961.

References

Balieiro, A. M., Anunciação, E. L., Costa, C. H., Qayed, W. S., & Silva, J. R. A. (2022). Computational

575 Analysis of SAM Analogs as Methyltransferase Inhibitors of nsp16/nsp10 Complex from
576 SARS-CoV-2. *International Journal of Molecular Sciences*, *23*(22), 13972.
577 Banerjee, A. K., Blanco, M. R., Bruce, E. A., Honson, D. D., Chen, L. M., Chow, A., Bhat, P., Ollikainen,
578 N., Quinodoz, S. A., & Loney, C. (2020). SARS-CoV-2 disrupts splicing, translation, and
579 protein trafficking to suppress host defenses. *Cell*, *183*(5), 1325-1339. e1321.
580 Bonamassa, B., Hai, L., & Liu, D. (2011). Hydrodynamic gene delivery and its applications in
581 pharmaceutical research. *Pharm Res*, *28*(4), 694-701. https://doi.org/10.1007/s11095-
582 010-0338-9
583 Cai, B., Zhao, J., Zhang, Y., Liu, Y., Ma, C., Yi, F., Zheng, Y., Zhang, L., Chen, T., & Liu, H. (2022). USP5
584 attenuates NLRP3 inflammasome activation by promoting autophagic degradation of
585 NLRP3. *Autophagy*, *18*(5), 990-1004.
586 Chen, X., Tian, L., Zhang, L., Gao, W., Yu, M., Li, Z., & Zhang, W. (2024). Deubiquitinase USP39
587 promotes SARS-CoV-2 replication by deubiquitinating and stabilizing the envelope
588 protein. *Antiviral Res*, *221*, 105790. https://doi.org/10.1016/j.antiviral.2023.105790
589 Decroly, E., Debarnot, C., Ferron, F., Bouvet, M., Coutard, B., Imbert, I., Gluais, L., Papageorgiou, N.,
590 Sharff, A., & Bricogne, G. (2011). Crystal structure and functional analysis of the SARS-
591 coronavirus RNA cap 2′-O-methyltransferase nsp10/nsp16 complex. *PLoS pathogens*,
592 *7*(5), e1002059.
593 Fan, L., Zhou, Y., Wei, X., Feng, W., Guo, H., Li, Y., Gao, X., Zhou, J., Wen, Y., Wu, Y., Shen, X., Liu, L.,
594 Xu, G., & Zhang, Z. (2024). The E3 ligase TRIM22 restricts SARS-CoV-2 replication by
595 promoting proteasomal degradation of NSP8. *mBio*, *15*(2), e0232023.
596 https://doi.org/10.1128/mbio.02320-23
597 Gao, W., Wang, L., Cui, W., Wang, H., Huang, G., Li, Z., Li, G., & Zhang, W. (2024). Deubiquitinase
598 USP1 regulates sarbecovirus ORF6 protein function. *J Virol*, *98*(1), e0143723.
599 https://doi.org/10.1128/jvi.01437-23
600 Gao, W., Wang, L., Ju, X., Zhao, S., Li, Z., Su, M., Xu, J., Wang, P., Ding, Q., & Lv, G. (2022). The
601 deubiquitinase USP29 promotes SARS-CoV-2 virulence by preventing proteasome
602 degradation of ORF9b. *Mbio*, *13*(3), e01300-01322.
603 [Record #31 is using a reference type undefined in this output style.]
604 Grice, G. L., & Nathan, J. A. (2016). The recognition of ubiquitinated proteins by the proteasome.
605 *Cellular and molecular life sciences*, *73*, 3497-3506.
606 Guo, G., Gao, M., Gao, X., Zhu, B., Huang, J., Luo, K., Zhang, Y., Sun, J., Deng, M., & Lou, Z. (2021).
607 SARS-CoV-2 non-structural protein 13 (nsp13) hijacks host deubiquitinase USP13 and
608 counteracts host antiviral immune response. *Signal transduction and targeted therapy*,
609 *6*(1), 119.
610 Hojyo, S., Uchida, M., Tanaka, K., Hasebe, R., Tanaka, Y., Murakami, M., & Hirano, T. (2020). How
611 COVID-19 induces cytokine storm with high mortality. *Inflamm Regen*, *40*, 37.
612 https://doi.org/10.1186/s41232-020-00146-3
613 Hu, B., Huang, S., & Yin, L. (2021). The cytokine storm and COVID-19. *J Med Virol*, *93*(1), 250-256.
614 https://doi.org/10.1002/jmv.26232
615 Ju, X., Zhu, Y., Wang, Y., Li, J., Zhang, J., Gong, M., Ren, W., Li, S., Zhong, J., Zhang, L., Zhang, Q. C.,
616 Zhang, R., & Ding, Q. (2021). A novel cell culture system modeling the SARS-CoV-2 life
617 cycle. *PLoS Pathog*, *17*(3), e1009439. https://doi.org/10.1371/journal.ppat.1009439
618 Kamimura, K., Kanefuji, T., Yokoo, T., Abe, H., Suda, T., Kobayashi, Y., Zhang, G., Aoyagi, Y., & Liu,

619 D. (2014). Safety assessment of liver-targeted hydrodynamic gene delivery in dogs. *PLoS*
620 *One*, *9*(9), e107203. https://doi.org/10.1371/journal.pone.0107203
621 Kim, J. G., Shin, H.-C., Seo, T., Nawale, L., Han, G., Kim, B. Y., Kim, S. J., & Cha-Molstad, H. (2021).
622 Signaling pathways regulated by UBR box-containing E3 ligases. *International journal of*
623 *molecular sciences*, *22*(15), 8323.
624 Klima, M., Khalili Yazdi, A., Li, F., Chau, I., Hajian, T., Bolotokova, A., Kaniskan, H. Ü., Han, Y., Wang,
625 K., & Li, D. (2022). Crystal structure of SARS-CoV-2 nsp10–nsp16 in complex with small
626 molecule inhibitors, SS148 and WZ16. *Protein Science*, *31*(9), e4395.
627 Li, Z., Hao, P., Zhao, Z., Gao, W., Huan, C., Li, L., Chen, X., Wang, H., Jin, N., & Luo, Z.-Q. (2023).
628 The E3 ligase RNF5 restricts SARS-CoV-2 replication by targeting its envelope protein for
629 degradation. *Signal Transduction and Targeted Therapy*, *8*(1), 53.
630 Liang, X., Xiao, J., Li, X., Liu, Y., Lu, Y., Wen, Y., Li, Z., Che, X., Ma, Y., & Zhang, X. (2022). A C-terminal
631 glutamine recognition mechanism revealed by E3 ligase TRIM7 structures. *Nature*
632 *Chemical Biology*, *18*(11), 1214-1223.
633 Lin, S., Chen, H., Ye, F., Chen, Z., Yang, F., Zheng, Y., Cao, Y., Qiao, J., Yang, S., & Lu, G. (2020).
634 Crystal structure of SARS-CoV-2 nsp10/nsp16 2′-O-methylase and its implication on
635 antiviral drug design. *Signal transduction and targeted therapy*, *5*(1), 131.
636 Lugari, A., Betzi, S., Decroly, E., Bonnaud, E., Hermant, A., Guillemot, J.-C., Debarnot, C., Borg, J.-P.,
637 Bouvet, M., & Canard, B. (2010). Molecular mapping of the RNA Cap 2′-O-
638 methyltransferase activation interface between severe acute respiratory syndrome
639 coronavirus nsp10 and nsp16. *Journal of Biological Chemistry*, *285*(43), 33230-33241.
640 Mahajan, S., Sharma, G. K., Bora, K., & Pattnaik, B. (2021). Identification of novel interactions
641 between host and non-structural protein 2C of foot-and-mouth disease virus. *J Gen Virol*,
642 *102*(3). https://doi.org/10.1099/jgv.0.001577
643 Maimaitiyiming, Y., Yang, T., Wang, Q. Q., Feng, Y., Chen, Z., Björklund, M., Wang, F., Hu, C., Hsu,
644 C.-H., & Naranmandura, H. (2022). Heat treatment promotes ubiquitin-mediated
645 proteolysis of SARS-CoV-2 RNA polymerase and decreases viral load. *Research*.
646 Makaremi, S., Asgarzadeh, A., Kianfar, H., Mohammadnia, A., Asghariazar, V., & Safarzadeh, E.
647 (2022). The role of IL-1 family of cytokines and receptors in pathogenesis of COVID-19.
648 *Inflamm Res*, *71*(7-8), 923-947. https://doi.org/10.1007/s00011-022-01596-w
649 McClellan, A. J., Laugesen, S. H., & Ellgaard, L. (2019). Cellular functions and molecular mechanisms
650 of non-lysine ubiquitination. *Open Biology*, *9*(9), 190147.
651 Melo-Filho, C. C., Bobrowski, T., Martin, H.-J., Sessions, Z., Popov, K. I., Moorman, N. J., Baric, R. S.,
652 Muratov, E. N., & Tropsha, A. (2022). Conserved coronavirus proteins as targets of broad-
653 spectrum antivirals. *Antiviral Research*, *204*, 105360.
654 Muñoz-Escobar, J., Matta-Camacho, E., Kozlov, G., & Gehring, K. (2015). The MLLE domain of the
655 ubiquitin ligase UBR5 binds to its catalytic domain to regulate substrate binding. *Journal*
656 *of Biological Chemistry*, *290*(37), 22841-22850.
657 Nathan, J. A., Sengupta, S., Wood, S. A., Admon, A., Markson, G., Sanderson, C., & Lehner, P. J.
658 (2008). The ubiquitin E3 ligase MARCH7 is differentially regulated by the deubiquitylating
659 enzymes USP7 and USP9X. *Traffic*, *9*(7), 1130-1145.
660 Park, G. J., Osinski, A., Hernandez, G., Eitson, J. L., Majumdar, A., Tonelli, M., Henzler-Wildman, K.,
661 Pawłowski, K., Chen, Z., & Li, Y. (2022). The mechanism of RNA capping by SARS-CoV-2.
662 *Nature*, *609*(7928), 793-800.

663 Qiao, X., Liu, Y., Prada, M. L., Mohan, A. K., Gupta, A., Jaiswal, A., Sharma, M., Merisaari, J., Haikala,
664 H. M., & Talvinen, K. (2020). UBR5 is coamplified with MYC in breast tumors and encodes
665 an ubiquitin ligase that limits MYC-dependent apoptosis. *Cancer research*, *80*(7), 1414-
666 1427.
667 Raper, S. E., Chirmule, N., Lee, F. S., Wivel, N. A., Bagg, A., Gao, G. P., Wilson, J. M., & Batshaw, M.
668 L. (2003). Fatal systemic inflammatory response syndrome in a ornithine transcarbamylase
669 deficient patient following adenoviral gene transfer. *Mol Genet Metab*, *80*(1-2), 148-158.
670 https://doi.org/10.1016/j.ymgme.2003.08.016
671 Rosas-Lemus, M., Minasov, G., Shuvalova, L., Inniss, N. L., Kiryukhina, O., Brunzelle, J., & Satchell,
672 K. J. (2020). High-resolution structures of the SARS-CoV-2 2′-O-methyltransferase reveal
673 strategies for structure-based inhibitor design. *Science signaling*, *13*(651), eabe1202.
674 Russ, A., Wittmann, S., Tsukamoto, Y., Herrmann, A., Deutschmann, J., Lagisquet, J., Ensser, A., Kato,
675 H., & Gramberg, T. (2022). Nsp16 shields SARS–CoV-2 from efficient MDA5 sensing and
676 IFIT1-mediated restriction. *EMBO reports*, *23*(12), e55648.
677 Shearer, R. F., Frikstad, K.-A. M., McKenna, J., McCloy, R. A., Deng, N., Burgess, A., Stokke, T., Patzke,
678 S., & Saunders, D. N. (2018). The E3 ubiquitin ligase UBR5 regulates centriolar satellite
679 stability and primary cilia. *Molecular biology of the cell*, *29*(13), 1542-1554.
680 Song, P., Li, W., Xie, J., Hou, Y., & You, C. (2020). Cytokine storm induced by SARS-CoV-2. *Clin*
681 *Chim Acta*, *509*, 280-287. https://doi.org/10.1016/j.cca.2020.06.017
682 Suda, T., Yokoo, T., Kanefuji, T., Kamimura, K., Zhang, G., & Liu, D. (2023). Hydrodynamic Delivery:
683 Characteristics, Applications, and Technological Advances. *Pharmaceutics*, *15*(4).
684 https://doi.org/10.3390/pharmaceutics15041111
685 Wu, B., Song, M., Dong, Q., Xiang, G., Li, J., Ma, X., & Wei, F. (2022). UBR5 promotes tumor immune
686 evasion through enhancing IFN-γ-induced PDL1 transcription in triple negative breast
687 cancer. *Theranostics*, *12*(11), 5086.
688 Xiang, G., Wang, S., Chen, L., Song, M., Song, X., Wang, H., Zhou, P., Ma, X., & Yu, J. (2022). UBR5
689 targets tumor suppressor CDC73 proteolytically to promote aggressive breast cancer. *Cell*
690 *Death & Disease*, *13*(5), 451.
691 Xu, G., Wu, Y., Xiao, T., Qi, F., Fan, L., Zhang, S., Zhou, J., He, Y., Gao, X., & Zeng, H. (2022).
692 Multiomics approach reveals the ubiquitination-specific processes hijacked by SARS-
693 CoV-2. *Signal Transduction and Targeted Therapy*, *7*(1), 312.
694 Zhang, H., Zheng, H., Zhu, J., Dong, Q., Wang, J., Fan, H., Chen, Y., Zhang, X., Han, X., & Li, Q.
695 (2021). Ubiquitin-modified proteome of SARS-CoV-2-infected host cells reveals insights
696 into virus–host interaction and pathogenesis. *Journal of Proteome Research*, *20*(5), 2224-
697 2239.
698 Zhang, J., Cruz-Cosme, R., Zhuang, M.-W., Liu, D., Liu, Y., Teng, S., Wang, P.-H., & Tang, Q. (2020).
699 A systemic and molecular study of subcellular localization of SARS-CoV-2 proteins. *Signal*
700 *transduction and targeted therapy*, *5*(1), 269.
701 Zhang, L., Hao, P., Chen, X., Lv, S., Gao, W., Li, C., Li, Z., & Zhang, W. (2024). CRL4B E3 ligase
702 recruited by PRPF19 inhibits SARS-CoV-2 infection by targeting ORF6 for ubiquitin-
703 dependent degradation. *mBio*, *15*(2), e0307123. https://doi.org/10.1128/mbio.03071-23
704 Zhang, L., Wang, H., Tian, L., & Li, H. (2016). Expression of USP7 and MARCH7 is correlated with
705 poor prognosis in epithelial ovarian cancer. *The Tohoku journal of experimental medicine*,
706 *239*(3), 165-175.

Zhang, X., Yang, Z., Pan, T., Sun, Q., Chen, Q., Wang, P. H., Li, X., & Kuang, E. (2023). SARS-CoV-2 Nsp8 suppresses MDA5 antiviral immune responses by impairing TRIM4-mediated K63-linked polyubiquitination. *PLoS Pathog*, *19*(11), e1011792. https://doi.org/10.1371/journal.ppat.1011792

Zhao, K., Yang, Y., Zhang, G., Wang, C., Wang, D., Wu, M., & Mei, Y. (2018). Regulation of the Mdm2–p53 pathway by the ubiquitin E3 ligase MARCH 7. *EMBO reports*, *19*(2), 305-319.

Zheng, C. (2021). The emerging roles of the MARCH ligases in antiviral innate immunity. *International Journal of Biological Macromolecules*, *171*, 423-427.

Zhou, Y., Zheng, R., Liu, D., Liu, S., Disoma, C., Li, S., Liao, Y., Chen, Z., Du, A., & Dong, Z. (2022). UBR5 Acts as an Antiviral Host Factor against MERS-CoV via Promoting Ubiquitination and Degradation of ORF4b. *Journal of Virology*, *96*(17), e00741-00722.

Züst, R., Cervantes-Barragan, L., Habjan, M., Maier, R., Neuman, B. W., Ziebuhr, J., Szretter, K. J., Baker, S. C., Barchet, W., & Diamond, M. S. (2011). Ribose 2′-O-methylation provides a molecular signature for the distinction of self and non-self mRNA dependent on the RNA sensor Mda5. *Nature immunology*, *12*(2), 137-143.

Figure legends

Figure 1. The non-structural protein nsp16 of SARS-CoV-2 was identified that can be degraded through the proteasome pathway.

A. The non-structural proteins nsp8, nsp11 and nsp16 could be restored by the proteasome inhibitor MG132. HEK293T cells in 12-well plates were transfected with the plasmids of 16 nonstructural proteins (nsp1-16) encoded by SARS-CoV-2. Thirty-six hours later, the cells were treated with MG132 (10 μM) or DMSO for 12 h before collection. The protein level was detected by Immunoblotting (IB). Quantification of nsp protein levels relative to the control protein is shown. Data are representative of three independent experiments and shown as average ±SD (n = 3). Significance was determined by a two-tailed t-test: *P < 0.05; **P < 0.01; ***P < 0.001.

B. Proteasomal inhibitors but no other inhibitors stabilized nsp16 protein. HEK293T cells transfected with the nsp16-Flag expression vector were treated with dimethyl sulfoxide (DMSO), MG132 (10 μM), Bortezomib (10 μM), Carfilzomib (10 μM), Bafilomycin A1 (5 μM), Vinblastine (2.5 μM), or NH_4CL (2.5 μM) for 12 h prior to harvest. The cell lysates were analyzed by anti-Flag antibody.

(C-D). The half-life of nsp16 was prolonged by the proteasome inhibitor MG132. C. HEK293T cells were transfected with the nsp16-Flag-expressing plasmids. 12 hours later, the cells were treated with DMSO or MG132 (10 μM) for 12 h, then 50 μg/mL cycloheximide (CHX) was added. Cells were harvested at the indicated times to detect the level of viral protein by anti-Flag antibody. D. Quantification of nsp16 protein levels relative to tubulin at different time points is shown. The half-life of the nsp16 protein was determined based on protein quantification using Image J, combined with the protein half-life formula for calculation. Results are shown as mean ± SD (n = 3 independent experiments). ***, P < 0.001 by by a two-tailed t-test.

E. Samples were prepared for mass spectrometry, and nsp16 interacting proteins were obtained by immunoprecipitation (IP) (created with BioRender.com and the agreement no. is LC27PCBEOF). The plasmids were transfected into HEK293T cells for 48 h. Treat cells

with or without MG132 (10 μM) for 12 h prior to harvest. The whole-cell lysates were incubated with protein G agarose beads conjugated with anti-Flag antibodies and used for IB with anti-Flag antibodies to detect the nsp16 protein. Samples enriched for proteins were analyzed by mass spectrometry.

Figure 1—figure supplement 1. Analysis of mass spectrometry results.

A. The DAVID bioinformatics website (https://david.ncifcrf.gov/tools.jsp) was used for KEGG pathway analysis and GO analysis of the differential proteins bound by nsp16 protein after treating with or without MG132. The bubble plots or circle diagram depict the results of the analysis separately. In bubble plots, a change from yellow to purple indicates a decreased p-value, while the size of the circles indicates the number of enriched genes. In the circle plot, depicting the BP (Biological process) analysis in the GO term, the length of the purple rectangle indicates the number of genes included in the term. The length of the green rectangle indicates the number of overlapping genes between the genes included in the term and the genes entered in the gene enrichment analysis, a change from deep to shallow of purple indicates a decreased p-value (created with chiplot.com).

B. Schematic representation of proteins degraded by the proteasome pathway, as well as proteins associated with the proteasome in the MS enrichment analysis are shown (created with BioRender.com and the agreement no. is VO27O5XHHC).

Figure 2. MARCHF7 and UBR5 were identified as E3 ubiquitin ligases involves in nsp16 protein degradation.

A. Knockdown of MARCHF7 or UBR5 resulted in nsp16 restoration. HEK293T cells were transfected with siRNA of E3 ligase candidates for 24 h, followed by co-incubation with the nsp16-Flag-expressing plasmids for 48 h, treated with MG132 (10 μM) for 16h before harvesting, lysed, and subjected to IB assay using anti-Flag antibody. RT-qPCR was conducted to determine the mRNA expression levels of E3 ligase candidates. The si-RNA targeting regions for the candidate E3 ubiquitin ligase proteins and the targeted regions for RT-qPCR are shown in Appendix-figure S1A. Data are representative of three independent experiments and shown as average ± SD (n = 3). Significance was determined by a two-

tailed t-test: ***P < 0.001.

B. RNA levels of UBR5 or MARCHF7 from HEK293T cells infected with lentivirus containing control or shRNA targeting UBR5 or MARCHF7 for 48 h and screened with antibiotics for 48 h. Knockdown cell lines were transfected with plasmids expressing nsp16-Flag, collected at the indicated times, and the protein levels of nsp16, MARCHF7, and UBR5 were detected by IB.C. MARCHF7 and UBR5 acted separately and did not depend on each other. HEK293T cells stably expressing UBR5 shRNA or MARCHF7 shRNA were transfected with siRNA of MARCHF7 or UBR5 for 24 h, respectively, followed by co-incubation with the nsp16-Flag-expressing plasmids for 48 h. The protein levels and the RNA levels of nsp16, UBR5 and MARCHF7 were measured by IB and RT-qPCR, respectively.

(D-E). In HEK293T cells stably expressing UBR5 shRNA or MARCHF7 shRNA, nsp16 was degraded by overexpressed UBR5 or MARCHF7, respectively, whereas the mutant failed to degrade nsp16. The cell lysates were analyzed by anti-Flag antibody.

Figure 2—figure supplement 1. MARCHF7 and UBR5 degrade nsp16 independently.

(A-B). UBR5 siRNA was transfected into shMARCHF7 cells to knock down UBR5. After 24 hours, MARCHF7 and nsp16 expression vectors were co-transfected, and the cells were harvested 72 hours later. The levels of nsp16 were characterized by IB with anti-Flag antibody. Whether MARCHF7 was dependent on UBR5 to degrade of nsp16 was determined by further transfection of MARCHF7 siRNA into shUBR5 cells, followed by co-transfection of UBR5 and nsp16 expression vectors 24 h later. The other operations are the same as above. Data are representative of three independent experiments and shown as average ±SD (n = 3). Significance was determined by a two-tailed t-test. *P > 0.05; **P < 0.01; ***P < 0.001.

Figure 3. MARCHF7 or UBR5 catalyze the formation of K-27 type or K-48 type ubiquitin chains of nsp16 respectively.

A. Nsp16 can be ubiquitinated. HEK293T cells co-transfected with ubiquitin-Myc and nsp16-Flag or transfected with nsp16-Flag alone. The cells were treated with MG132 for

12 h before collection. The whole-cell lysates were incubated with anti-Flag beads and used for IB with anti-Myc or anti-Flag antibodies to detect the polyubiquitination chain of nsp16.

B. Assess the endogenous ubiquitination level of nsp16 protein. Cells were transfected with nsp16-Flag or an empty vector, and collected 48 hours later. Prior to harvesting, cells were treated with MG132 for 16 hours. Co-IP experiments were then performed to analyze the endogenous ubiquitination level of nsp16.

C. The level of ubiquitination of nsp16 decreased with decreasing the protein levels of MARCHF7 or UBR5. E3 was knocked down by transfection with siRNA targeting UBR5 or MARCHF7, and 24 h later ubiquitin-Myc and nsp16-HA were co-transfected or nsp16-HA alone. Cells were treated with MG132 for 16 h before collection. Whole cell lysates were incubated with anti-HA beads, and polyubiquitinated chains of nsp16 were detected by IB with anti-Myc or anti-HA antibodies.

D. Nsp16 can be modified by a variety of ubiquitin chains. HEK293T cells were transfected with either nsp16-HA alone or together with plasmids encoding various mutants of ubiquitin (K6 only, K11 only, K27 only, K29 only, K33 only, K48 only, K63 only). Thirty-six hours later, cells were treated with MG132 for 12 h. Cell lysates were then subjected to immunoprecipitation, followed by IB to analysis.

(E-F) MARCHF7 or UBR5 causes nsp16 to be modified by the K27 type or K48 type ubiquitin chain. 293T cell lines with or without MARCHF7 or UBR5 knockdown were co-transfected with plasmids encoding ubiquitin-WT or various mutants of ubiquitin (K6 only, K11 only, K27 only, K29 only, K33 only, K48 only, K63 only). The other experimental methods were the same as C.

Figure 4. MARCHF7 and UBR5 directly interact with nsp16 respectively.

(A-B). The binding of MARCHF7 or UBR5 to nsp16 was not mutually dependent. The binding of nsp16 to UBR5 or MARCHF7 was identified by co-immunoprecipitation in HEK293T cells transfected siMARCHF7 or siUBR5, respectively. The immunoprecipitates and input were analyzed by IB. The knockdown efficiency was detected by RT-qPCR and IB.

(C-D). MARCHF7 or UBR5 co-localized with nsp16 in the endoplasmic reticulum. Hela cells were co-transfected with YFP-nsp16(yellow) and CFP-UBR5(cyan) or CFP-MARCHF7(cyan). The organelles were labeled with antibodies against marker proteins of endoplasmic reticulum, Golgi apparatus and mitochondria respectively(red). The cells were analyzed by confocal microscopy (C). Scale bars, 20 um. The ratio of colocalization was quantified by measuring the fluorescence intensities using Image J (D).

Figure 4—figure supplement 1. Interaction of MARCHF7 or UBR5 with nsp16.

A. HEK293T cells were transfected with either nsp16-Flag alone or together with MARCHF7-Myc. Thirty-six hours after transfection, the cells were treated with MG132 (10 μM) for 12 h. Cell lysates were subjected to immunoprecipitation with anti-Flag antibody. Using IB to analyze the precipitates and input.

B. HEK293T cells were transfected with nsp16-Flag. Cell lysates were subjected to immunoprecipitation with anti-UBR5 or IgG antibody.

(C-D). Hela cells were co-transfected with YFP-nsp16 and CFP-UBR5 or CFP-MARCHF7. A representative image of YFP-nsp16 (yellow) and ECFP-MARCHF7 (cyan) or ECFP-UBR5 (cyan) expressing cells before and after photobleaching the acceptor fluorophore, YFP. The region chosen for photobleaching is marked (white open box), Bars, 10um. The quantization of fluorescence brightness was analyzed by Image J. Data are representative of three independent experiments and shown as average ±SD (n = 3). Significance was determined by a two-tailed t-test. *P > 0.05; **P < 0.01; ***P < 0.001.

E. HeLa cells transfected with nsp16-Flag were analyzed by confocal microscopy. The Flag-tagged nsp16 labeled with anti-Flag antibody (red). MARCHF7 or UBR5 were labeled with endogenous antibodies (green). Cell nuclei were stained using DAPI (blue). Representative images were shown. Scale bars, 20 um. The ratio of colocalization was quantified by measuring the fluorescence intensities using Image J.

F. nsp16 was stably transfected into HEK293T cells. The cells were analyzed by confocal microscopy. The other operations are the same as above.

Figure 4—figure supplement 2. Domains in which MARCHF7 or UBR5 functions.

A. The schematic represents UBR5 WT or mutants used in the study.

B. The HECT domain of UBR5 is required for nsp16 degradation. After co-transfection with UBR5 WT or mutants and nsp16-HA, cells were harvested 48 hours later, and cell lysates were examined by IB.

C. The HECT domain of UBR5 affects K48-type ubiquitin chain of nsp16.HEK293T cells were transfected with the assigned plasmids. After 36 hours, cells were treated with 10 μM MG132 for 12 hours, harvested, and cell lysates were incubated with protein G agarose beads conjugated with anti-HA antibodies. Cell lysates and precipitated samples were analyzed by IB.

D. The schematic represents wild-type and truncated forms of MARCHF7 used in the study.

E. Only MARCHF7 wild-type degraded nsp16.

F. The N-terminal region of MARCHF7 interacted with nsp16, and only the wild type could catalyze the K27-type ubiquitin chain of nsp16.

Figure 5. Knockdown of MARCHF7 or UBR5 promotes viral replication.

A. The virus-encoded nsp16 protein interacts with endogenous MARCHF7 and UBR5 and undergoes ubiquitination modification. In 293T-ACE2 cells, with or without Wuhan strain infection (MOI: 0.01), the medium was changed 2 hours post-infection, and cells were harvested 48 hours later, with MG132 treatment added 16 hours before harvesting. nsp16 protein was enriched using Protein-G beads coupled with the nsp16 antibody, and interactions and ubiquitination were analyzed by immunoblotting (IB) with endogenous antibodies against MARCHF7, UBR5, and ubiquitination.

(B-I). MARCHF7 and UBR5 were knocked down by siRNA in Caco2 cells. 24 h after transfection, the cells were infected with Wuhan strain (MOI:0.01) (C-E) or Omicron BA.1 strain (MOI: 0.001) (F-H), respectively. 2 h post infection, the supernatant was discarded, and the cells were cultured in DMEM containing 3% fetal bovine serum for 48 h. The mRNA levels of SARS-CoV-2 *M* and *E* genes in the cells (C, F) and *E* genes in supernatant (D, G) were detected by RT-qPCR and the viral titers in supernatant (E, H) were measured. The N protein levels of Wuhan or Omicron viruses were detected by IB (I). Knock-down efficiencies of MARCHF7 and UBR5 were detected by RT-qPCR or IB (B, I). Data are

representative of three independent experiments and shown as average ±SD (n = 3). Significance was determined by one-way ANOVA, followed by a Tukey multiple comparisons posttest: *P < 0.05; **P < 0.01; ***P < 0.001.

Figure 5—figure supplement 1. Effect of MARCHF7 or UBR5 on SARS-CoV-2 trVLP.

(A-B). Knocking down MARCHF7 or UBR5 enhances SARS-CoV-2 trVLP infectivity. MARCHF7 or UBR5 was knocked down by siRNA in Caco2 cells with stable expression of SARS-CoV-2 N protein. Twenty-four hours later, cells were infected with SARS-CoV-2 virus-like-particles (MOI:0.1), the medium was changed two hours after infection, and the eGFP-positive cells were detected by flow cytometry 48 hours later (A). Protein content was determined by RT-qPCR (B).

Figure 6. Increased levels of nsp16 rescued viral inhibition by UBR5 or MARCHF7'

(A-H) UBR5 or MARCHF7 was transfected in 293T cells stably overexpressed with ACE2, and the increased doses of nsp16-Flag was transfected simultaneously. After 24 h, the cells were infected with Wuhan strains. The mRNA levels of *M* and *E* genes of Wuhan strain in the cells (A, D) and *E* gene in supernatant (B, E) were detected by RT-qPCR, as well as the detection of viral titers in supernatant (C, F). The N protein of the virus and the overexpression efficiency was detected by IB (G, H). Data are representative of three independent experiments and shown as average ±SD (n = 3). Significance was determined by one-way ANOVA, followed by a Tukey multiple comparisons posttest. P > 0.05; **P < 0.01; ***P < 0.001. Figure 6—figure supplement 1 shows data related to infection with Omicron BA.1.

Figure 6—figure supplement 1. Effect of MARCHF7 or UBR5 on Omicron BA.1 infectivity.

(A-H). Showing data related to infection with Omicron BA.1. The experimental procedure was the same as Figure 6. Data are representative of three independent experiments and shown as average ±SD (n = 3). Significance was determined by one-way ANOVA, followed by a Tukey multiple comparisons posttest. P > 0.05; **P < 0.01; ***P < 0.001.

Figure 6—figure supplement 2. The enzyme activity-deficient mutants do not exhibit

antiviral activity, and overexpression of nsp16 does not promote viral replication.

(A-H) In 293T-ACE2 cells, the RING domain deletion mutant of MARCHF7 (MARCHF7-aa 1-542) or the HECT domain inactivated mutant of UBR5 (UBR5-ΔHECT) were transfected, along with a gradient of nsp16-Flag overexpression. The cells were infected with the Wuhan strain (MOI: 0.01), medium was changed 2 hours post-infection, and cells and supernatants were collected 48 hours after infection.

Figure 6—figure supplement 3. MARCHF7 or UBR5 have effects on mutant of nsp16 in different subtypes of SARS-CoV-2.

A. This diagram shows the mutation of nsp16 in different virus subtypes. The amino acids sequences of different SARS-CoV-2 strains were obtained from NCBI, and the amino acids sequences of nsp16 of different strains were compared by DNAMAN software.

B. Nsp16 mutants can still be regulated by MG132. The mutated nsp16 plasmids were transfected into HEK293T cells. After 36 hours of culture, cells were treated with 10 μm MG132 or DMSO, harvested 12 hours later, and cell lysates were examined by IB.

C. MARCHF7 or UBR5 can degrade nsp16 mutants. After transfecting MARCHF7 or UBR5 siRNA and the mutated nsp16 plasmids, the cells were harvested 48 h later. The cell lysates were detected by IB.

Figure 6—figure supplement 4. The expression level of MARCHF7 was negatively correlated with the viral titer, while the expression level of UBR5 was increased at low titer and decreased at high titer.

(A-C). The protein and mRNA levels of MARCHF7 or UBR5 upon infection with different titers. Endogenous MARCHF7 and UBR5 RNA levels were detected by RT-qPCR 48 hours after infection with different titers of Wuhan strain (MOI:0, 0.0001, 0.001, 0.01) or omicron BA.1 strain (MOI:0, 0.0001, 0.001). Protein levels were examined by IB.

D. The expression level of UBR5 was negatively correlated with the severity of the disease but MARCHF7 expression levels were not. PBMC cells were extracted from common, severe and critical COVID-19 patients. RT-qPCR was used to detect the mRNA level of UBR5 or MARCHF7 in patients. Significance was determined by one-way ANOVA,

followed by a Tukey multiple comparisons posttest. ns, P > 0.05; **P < 0.01; ***P < 0.001.

Figure 7. In a mouse infection model, overexpression of MARCHF7 or UBR5 exerted inhibitory effects on virus.

(A-G) BLAB/C mice were injected with the corresponding plasmids at 40ug/500ul via the high-pressure tail vein, followed by nasal inoculation with 50μl SARS-CoV-2 virus at a dosage of $10^{5.5}$ TCID50/mL (created with BioRender.com and the agreement no. is FO27O5X39A). IB was used to detect the expression of MARCHF7 or UBR5 in the lung tissues (B). Viral RNA loads in mouse lung tissues were detected by measuring the mRNA levels of the E genes by RT-qPCR (C). Lung tissue was collected, homogenized, and the residue was removed by centrifugation to collect the supernatant. The viral titer was then measured using the TCID50 method (D). Mouse body weight was monitored during the experimental period (E). Representative images of H&E staining of lungs of mice with different treatments. Magnification, ×40. Bars, 20 μm (F). The staining of viral N proteins. Magnification, ×63. Bars, 20 μm. n =3 in each group (G). RT-qPCR was used to measure the expression of cytokines and chemokines in the spleens of mice in each group (H). Statistical significance was analyzed using a one-way analysis of variance with Tukey's multiple comparisons test. (NS, no significance, *p < 0.05, **p < 0.01, ***p < 0.001).

Figure 8. Schematic diagram of MARCHF7 and UBR5 ubiquitinate the SARS-CoV-2 non-structural protein nsp16, leading to its degradation via the proteasomal pathway, thereby affecting viral replication (created with BioRender.com and the agreement no. is FM27O5ZS3U).

Figure 1

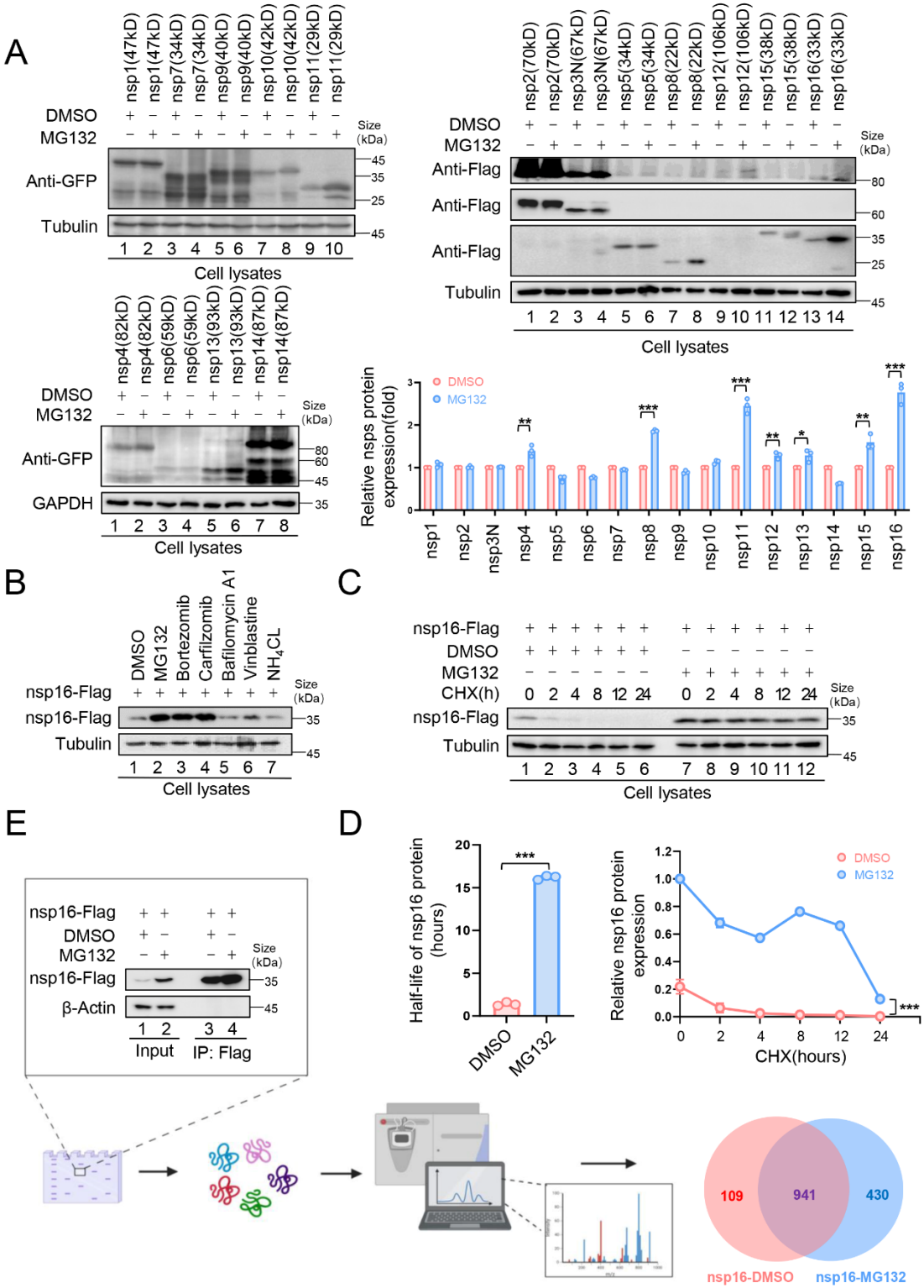
A
nsp1(47kD)
nsp1(47kD)
nsp7(34kD)
nsp7(34kD)
nsp9(40kD)
nsp9(40kD)
nsp10(42kD)
nsp10(42kD)
nsp11(29kD)
nsp11(29kD)
DMSO
MG132
Size (kDa)
Anti-GFP
Tubulin
45
35
25
45
1 2 3 4 5 6 7 8 9 10
Cell lysates
nsp2(70kD)
nsp2(70kD)
nsp3N(67kD)
nsp3N(67kD)
nsp5(34kD)
nsp5(34kD)
nsp8(22kD)
nsp8(22kD)
nsp12(106kD)
nsp12(106kD)
nsp15(38kD)
nsp15(38kD)
nsp16(33kD)
nsp16(33kD)
Anti-Flag
Anti-Flag
Anti-Flag
Tubulin
80
60
35
25
45
1 2 3 4 5 6 7 8 9 10 11 12 13 14
Cell lysates
nsp4(82kD)
nsp4(82kD)
nsp6(59kD)
nsp6(59kD)
nsp13(93kD)
nsp13(93kD)
nsp14(87kD)
nsp14(87kD)
Anti-GFP
GAPDH
80
60
45
35
1 2 3 4 5 6 7 8
Cell lysates
DMSO
MG132
Relative nsps protein expression(fold)
nsp1
nsp2
nsp3N
nsp4
nsp5
nsp6
nsp7
nsp8
nsp9
nsp10
nsp11
nsp12
nsp13
nsp14
nsp15
nsp16
B
DMSO
MG132
Bortezomib
Carfilzomib
Bafilomycin A1
Vinblastine
NH4CL
nsp16-Flag
nsp16-Flag
Tubulin
35
45
1 2 3 4 5 6 7
Cell lysates
C
nsp16-Flag
DMSO
MG132
CHX(h)
0 2 4 8 12 24 0 2 4 8 12 24
nsp16-Flag
Tubulin
35
45
1 2 3 4 5 6 7 8 9 10 11 12
Cell lysates
E
nsp16-Flag
DMSO
MG132
nsp16-Flag
β-Actin
35
45
1 2 3 4
Input
IP: Flag
D
Half-life of nsp16 protein (hours)
DMSO
MG132
Relative nsp16 protein expression
CHX(hours)
109
941
430
nsp16-DMSO
nsp16-MG132

Figure 1 supplement 1

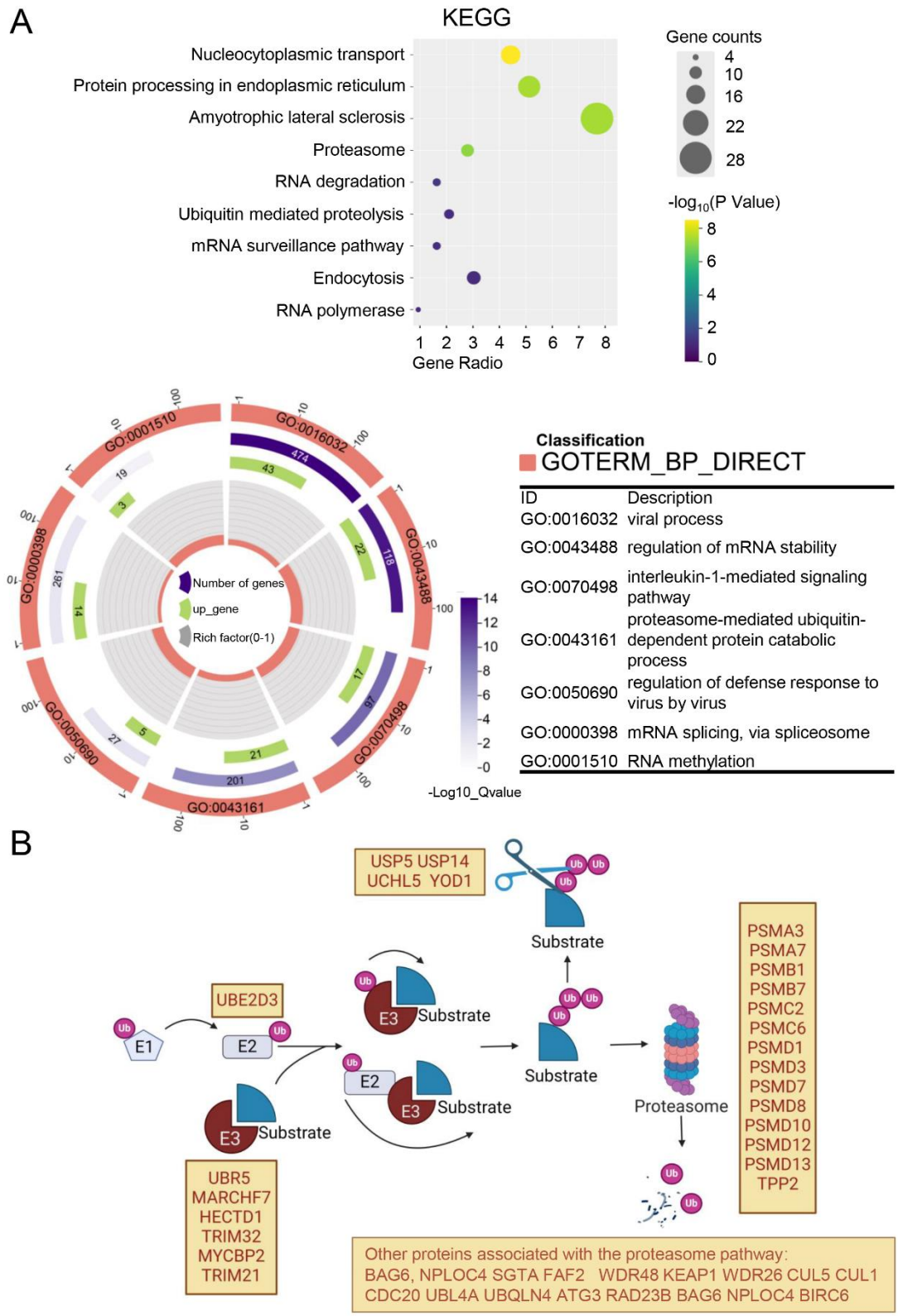

Figure 2

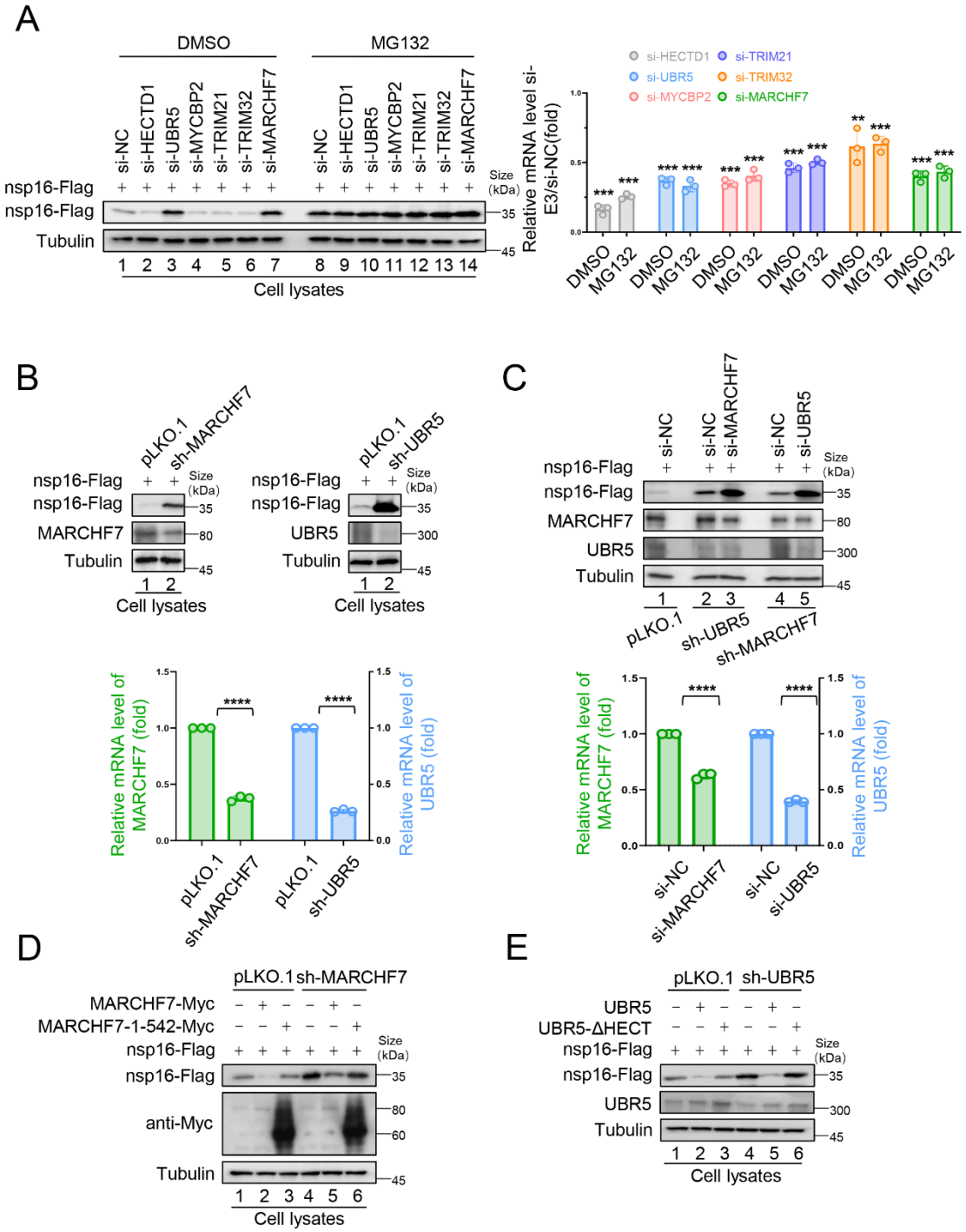
A
DMSO
MG132
si-NC
si-HECTD1
si-UBR5
si-MYCBP2
si-TRIM21
si-TRIM32
si-MARCHF7
nsp16-Flag
nsp16-Flag
Tubulin
Size (kDa)
35
45
1 2 3 4 5 6 7 8 9 10 11 12 13 14
Cell lysates
Relative mRNA level si-E3/si-NC(fold)
si-HECTD1
si-UBR5
si-MYCBP2
si-TRIM21
si-TRIM32
si-MARCHF7
DMSO
MG132
B
pLKO.1
sh-MARCHF7
sh-UBR5
nsp16-Flag
nsp16-Flag
MARCHF7
UBR5
Tubulin
35
80
300
45
1 2
Cell lysates
Relative mRNA level of MARCHF7 (fold)
Relative mRNA level of UBR5 (fold)
C
si-NC
si-MARCHF7
si-UBR5
nsp16-Flag
nsp16-Flag
MARCHF7
UBR5
Tubulin
1 2 3 4 5
pLKO.1
sh-UBR5
sh-MARCHF7
D
pLKO.1
sh-MARCHF7
MARCHF7-Myc
MARCHF7-1-542-Myc
nsp16-Flag
nsp16-Flag
anti-Myc
Tubulin
35
80
60
45
1 2 3 4 5 6
Cell lysates
E
pLKO.1
sh-UBR5
UBR5
UBR5-ΔHECT
nsp16-Flag
nsp16-Flag
UBR5
Tubulin
35
300
45
1 2 3 4 5 6
Cell lysates

Figure 2 supplement 1

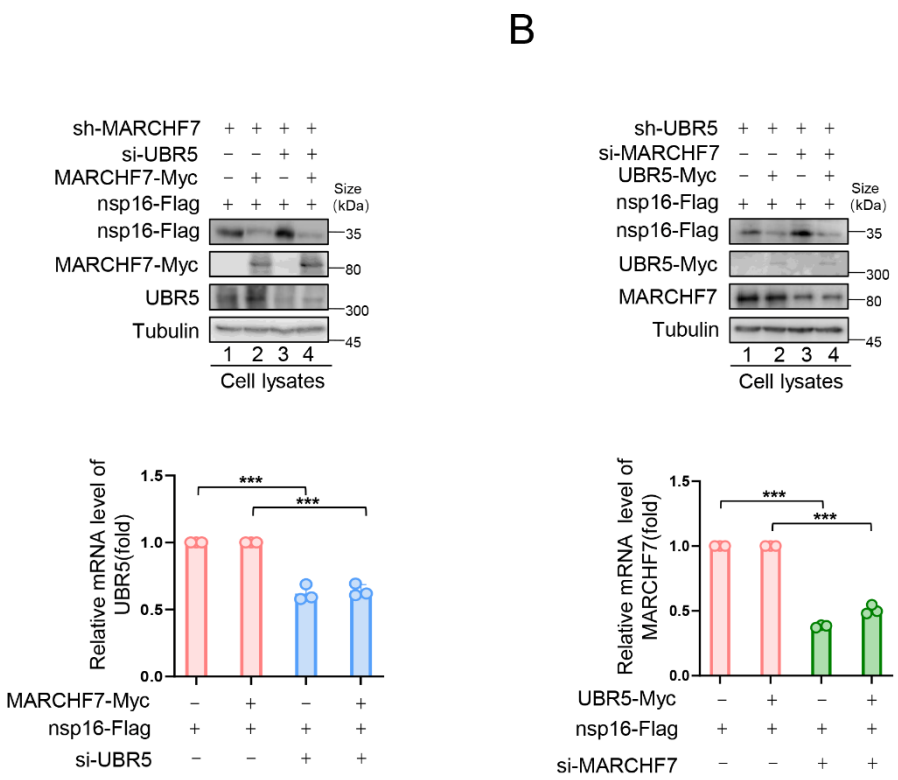

Figure 3

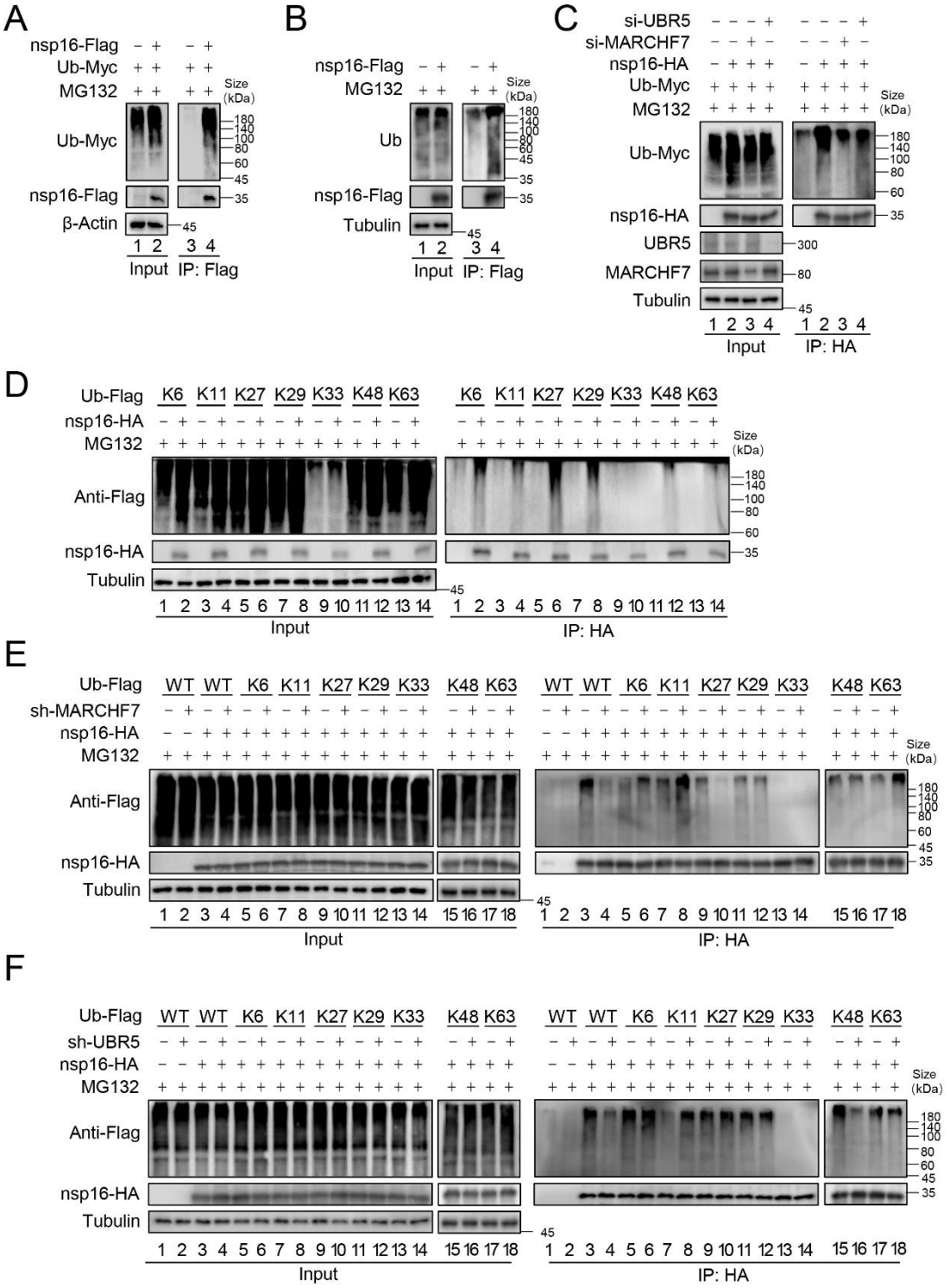
A
nsp16-Flag
Ub-Myc
MG132
Size (kDa)
Ub-Myc
nsp16-Flag
β-Actin
Input
IP: Flag
B
nsp16-Flag
MG132
Ub
nsp16-Flag
Tubulin
Input
IP: Flag
C
si-UBR5
si-MARCHF7
nsp16-HA
Ub-Myc
MG132
Ub-Myc
nsp16-HA
UBR5
MARCHF7
Tubulin
Input
IP: HA
D
Ub-Flag
K6 K11 K27 K29 K33 K48 K63
nsp16-HA
MG132
Anti-Flag
nsp16-HA
Tubulin
Input
IP: HA
E
Ub-Flag
WT WT K6 K11 K27 K29 K33 K48 K63
sh-MARCHF7
nsp16-HA
MG132
Anti-Flag
nsp16-HA
Tubulin
Input
IP: HA
F
Ub-Flag
WT WT K6 K11 K27 K29 K33 K48 K63
sh-UBR5
nsp16-HA
MG132
Anti-Flag
nsp16-HA
Tubulin
Input
IP: HA

Figure 4

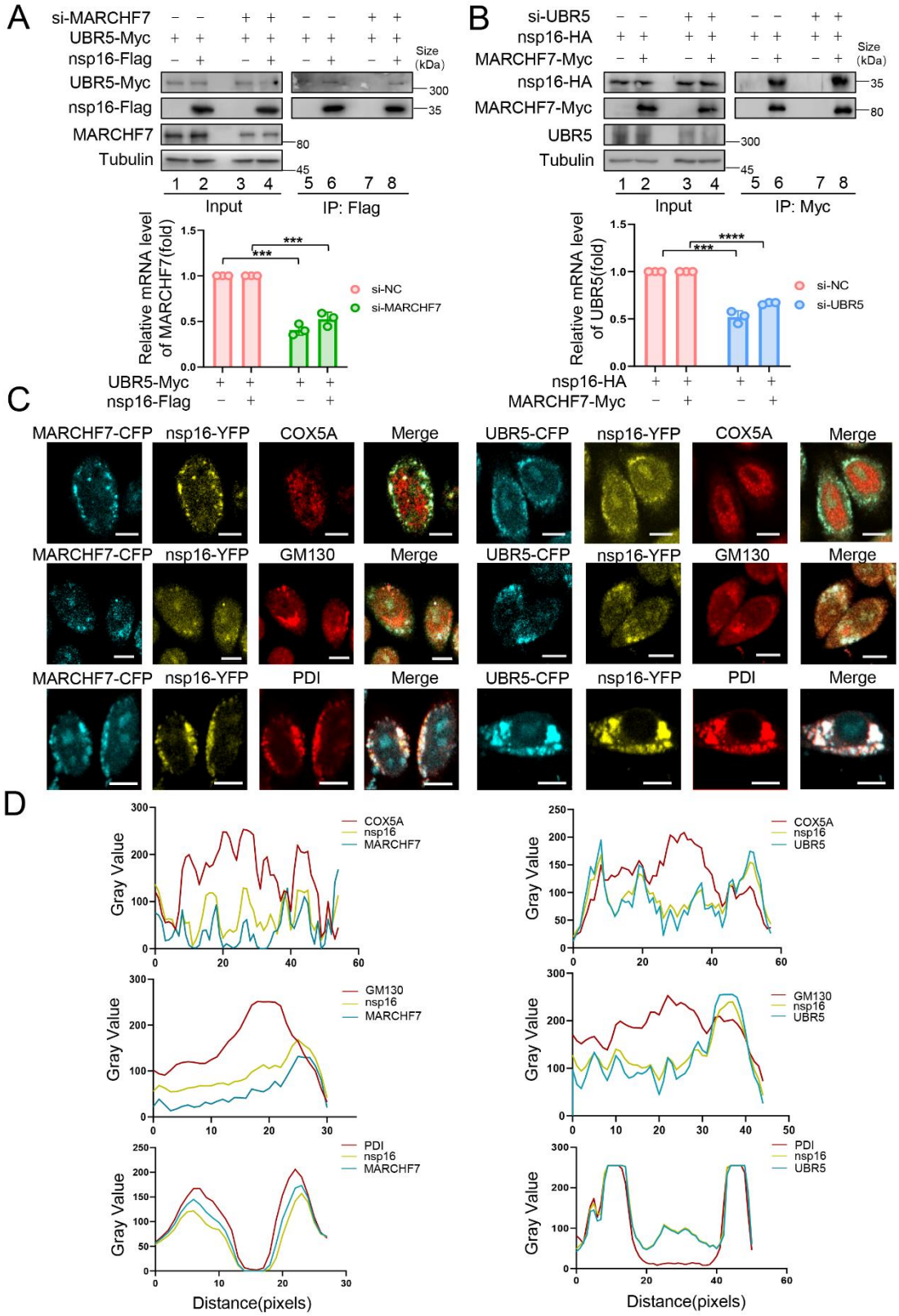
A
si-MARCHF7
UBR5-Myc
nsp16-Flag
UBR5-Myc
nsp16-Flag
MARCHF7
Tubulin
Size (kDa)
300
35
80
45
1 2 3 4 5 6 7 8
Input
IP: Flag
Relative mRNA level of MARCHF7(fold)
si-NC
si-MARCHF7
B
si-UBR5
nsp16-HA
MARCHF7-Myc
nsp16-HA
MARCHF7-Myc
UBR5
Tubulin
Input
IP: Myc
Relative mRNA level of UBR5(fold)
si-NC
si-UBR5
C
MARCHF7-CFP
nsp16-YFP
COX5A
GM130
PDI
Merge
UBR5-CFP
D
Gray Value
Distance(pixels)
COX5A
GM130
PDI
nsp16
MARCHF7
UBR5

Figure 4 supplement 1

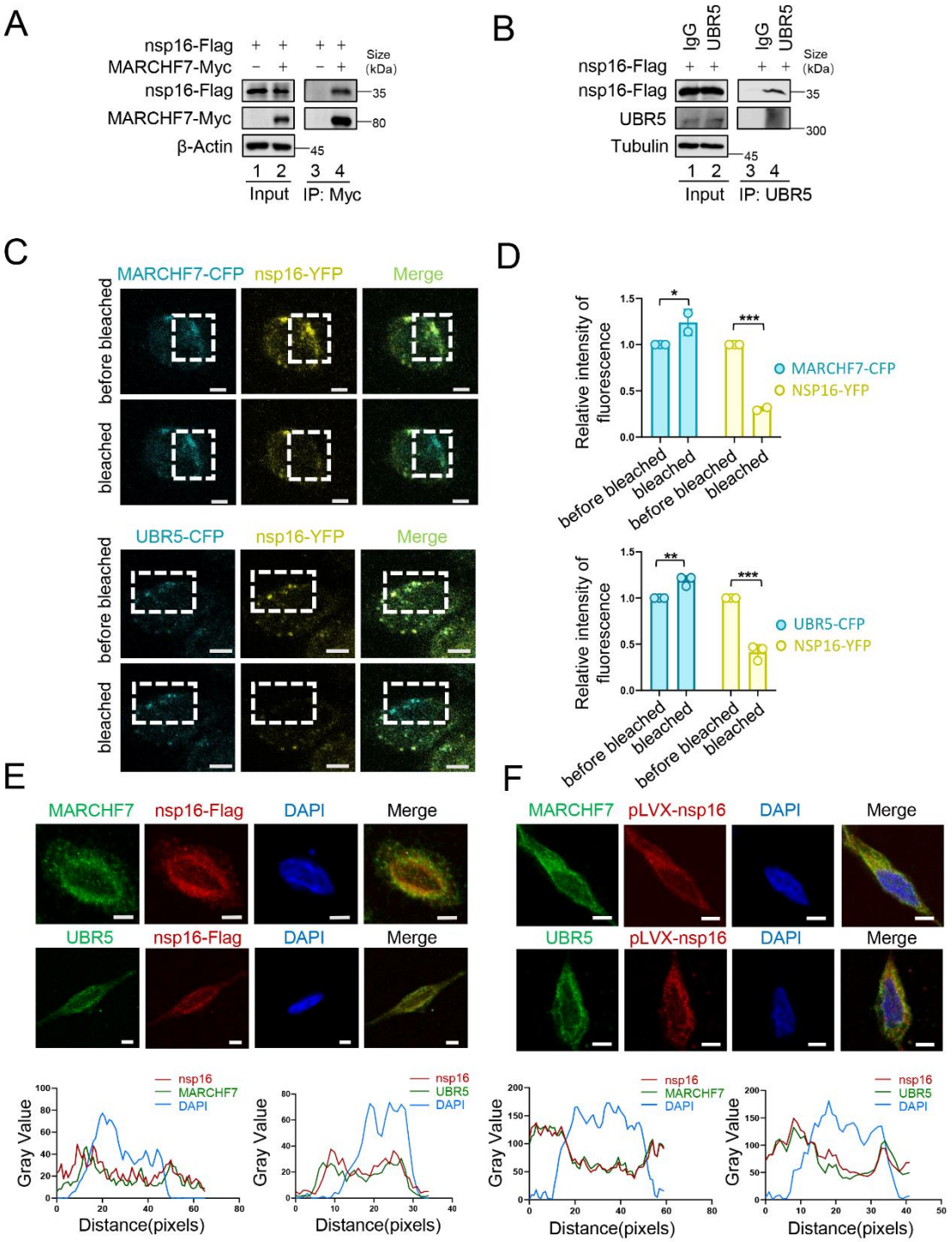

Figure 4 supplement 2

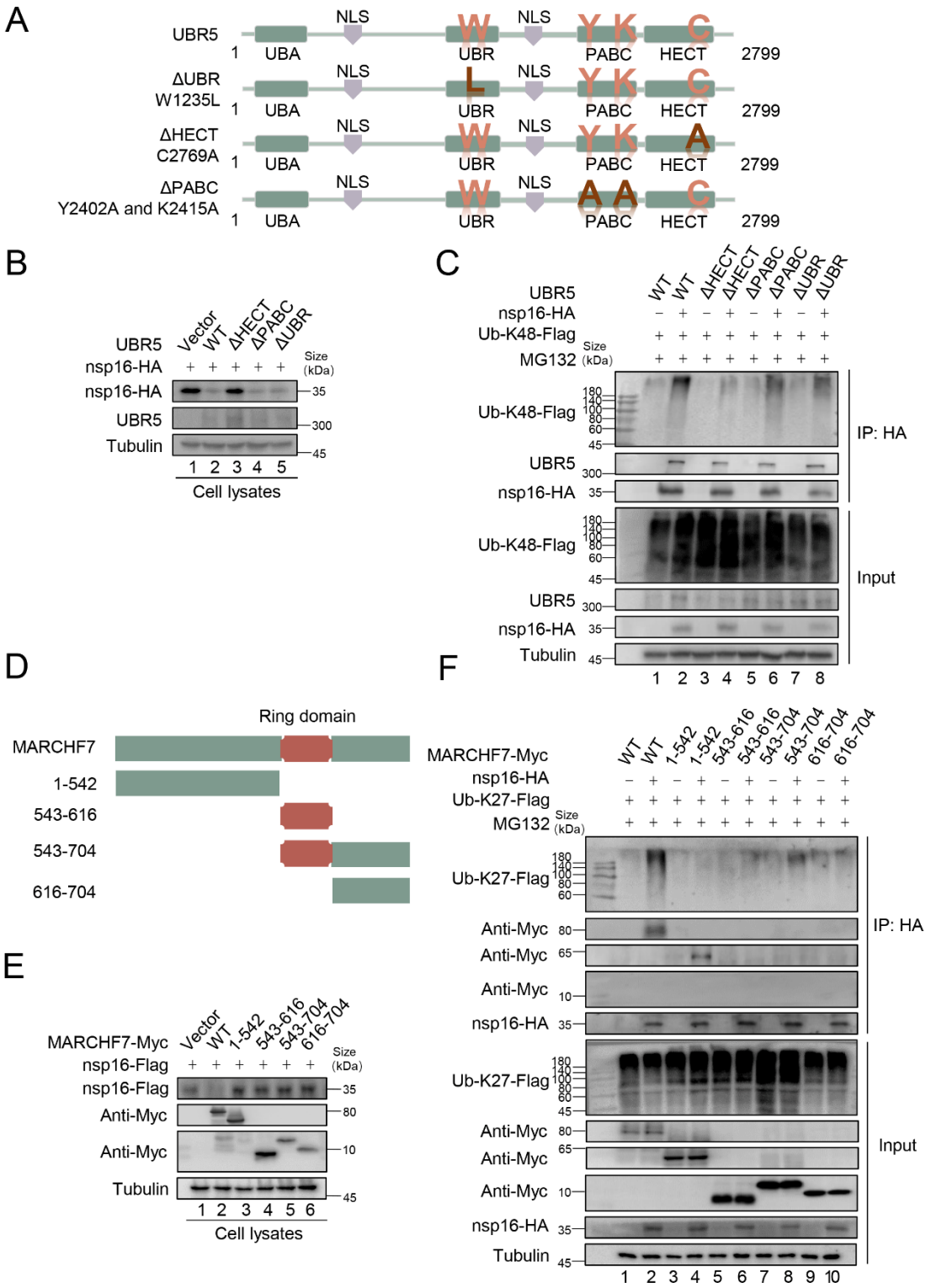

Figure 5

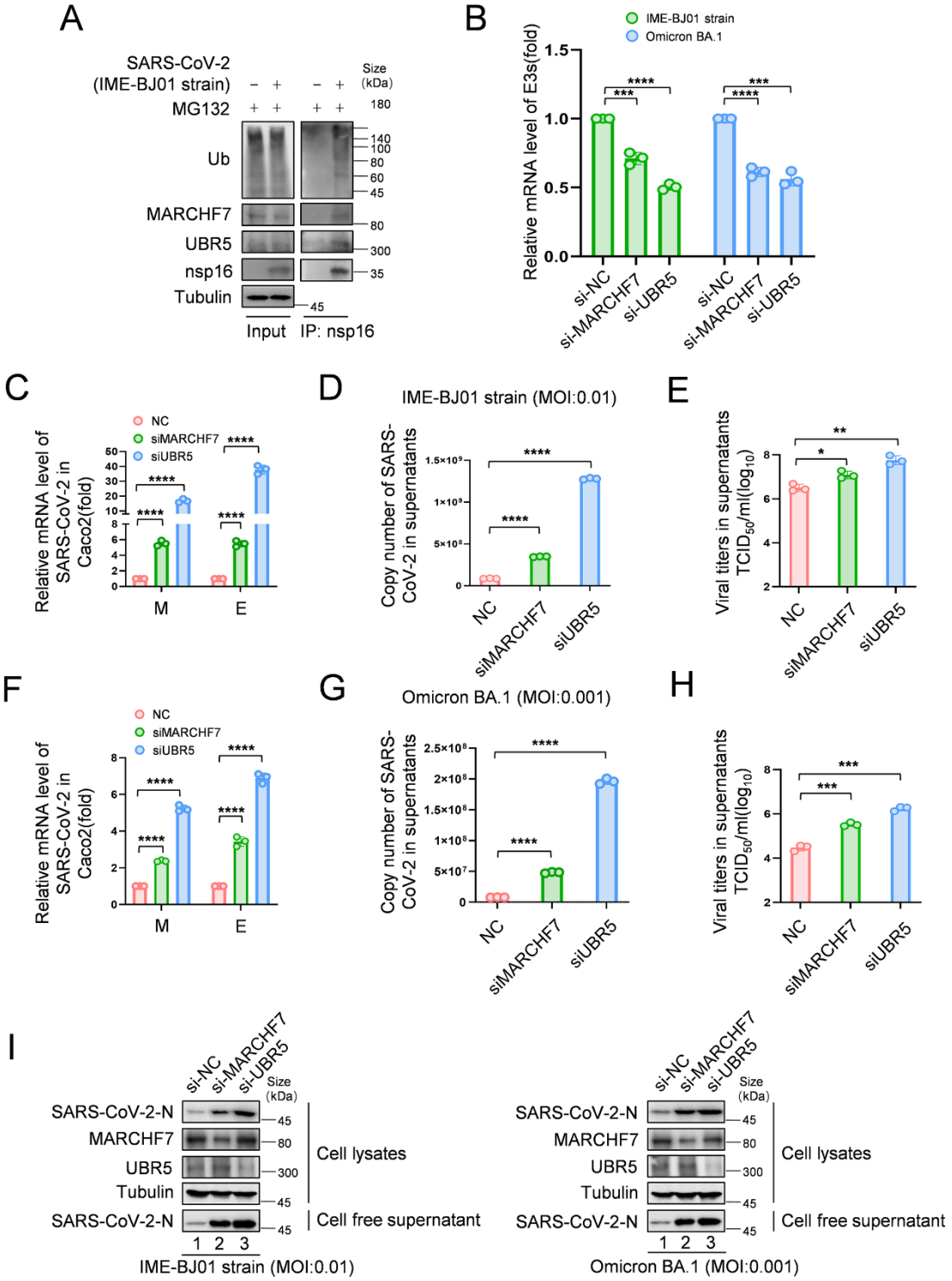
A
SARS-CoV-2 (IME-BJ01 strain)
MG132
Size (kDa)
Ub
MARCHF7
UBR5
nsp16
Tubulin
Input
IP: nsp16
B
IME-BJ01 strain
Omicron BA.1
Relative mRNA level of E3s(fold)
si-NC
si-MARCHF7
si-UBR5
C
NC
siMARCHF7
siUBR5
Relative mRNA level of SARS-CoV-2 in Caco2(fold)
M
E
D
IME-BJ01 strain (MOI:0.01)
Copy number of SARS-CoV-2 in supernatants
E
Viral titers in supernatants TCID50/ml(log10)
F
G
Omicron BA.1 (MOI:0.001)
H
I
Cell lysates
Cell free supernatant
IME-BJ01 strain (MOI:0.01)
Omicron BA.1 (MOI:0.001)

Figure 5 supplement 1

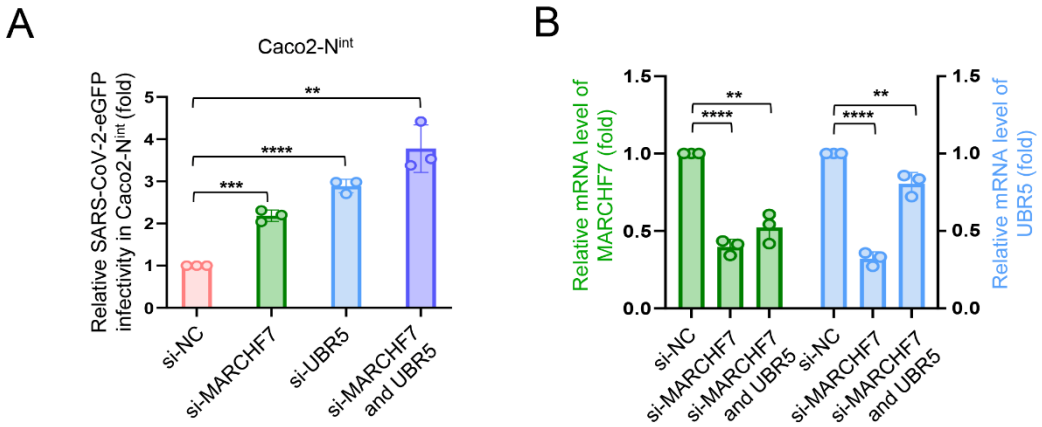

Figure 6

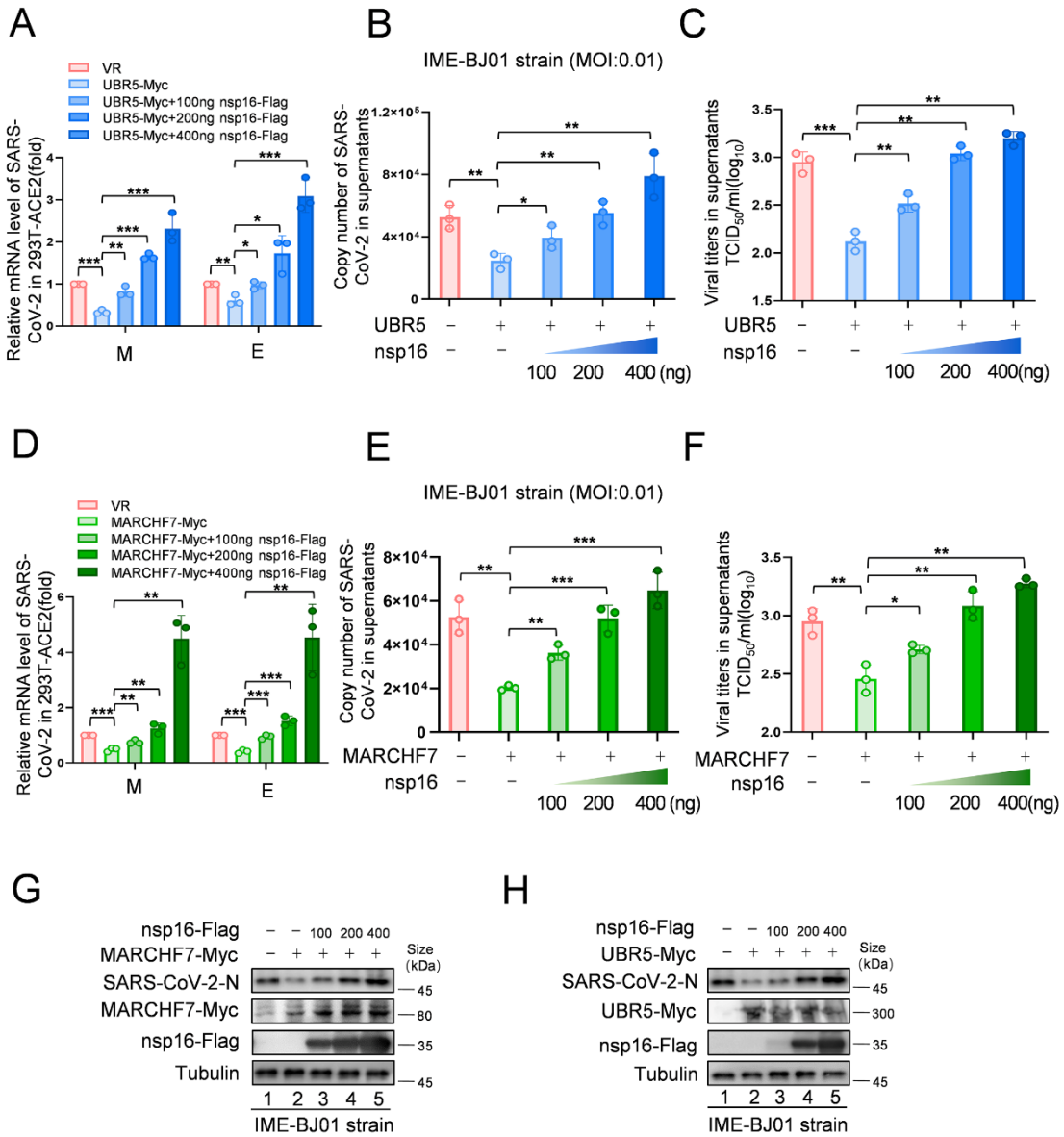
A
VR
UBR5-Myc
UBR5-Myc+100ng nsp16-Flag
UBR5-Myc+200ng nsp16-Flag
UBR5-Myc+400ng nsp16-Flag
Relative mRNA level of SARS-CoV-2 in 293T-ACE2(fold)
M
E
B
IME-BJ01 strain (MOI:0.01)
Copy number of SARS-CoV-2 in supernatants
UBR5
nsp16
100 200 400 (ng)
C
Viral titers in supernatants TCID50/ml(log10)
100 200 400(ng)
D
MARCHF7-Myc
MARCHF7-Myc+100ng nsp16-Flag
MARCHF7-Myc+200ng nsp16-Flag
MARCHF7-Myc+400ng nsp16-Flag
E
F
MARCHF7
G
nsp16-Flag
MARCHF7-Myc
SARS-CoV-2-N
Tubulin
Size (kDa)
IME-BJ01 strain
H
UBR5-Myc

Figure 6 supplement 1

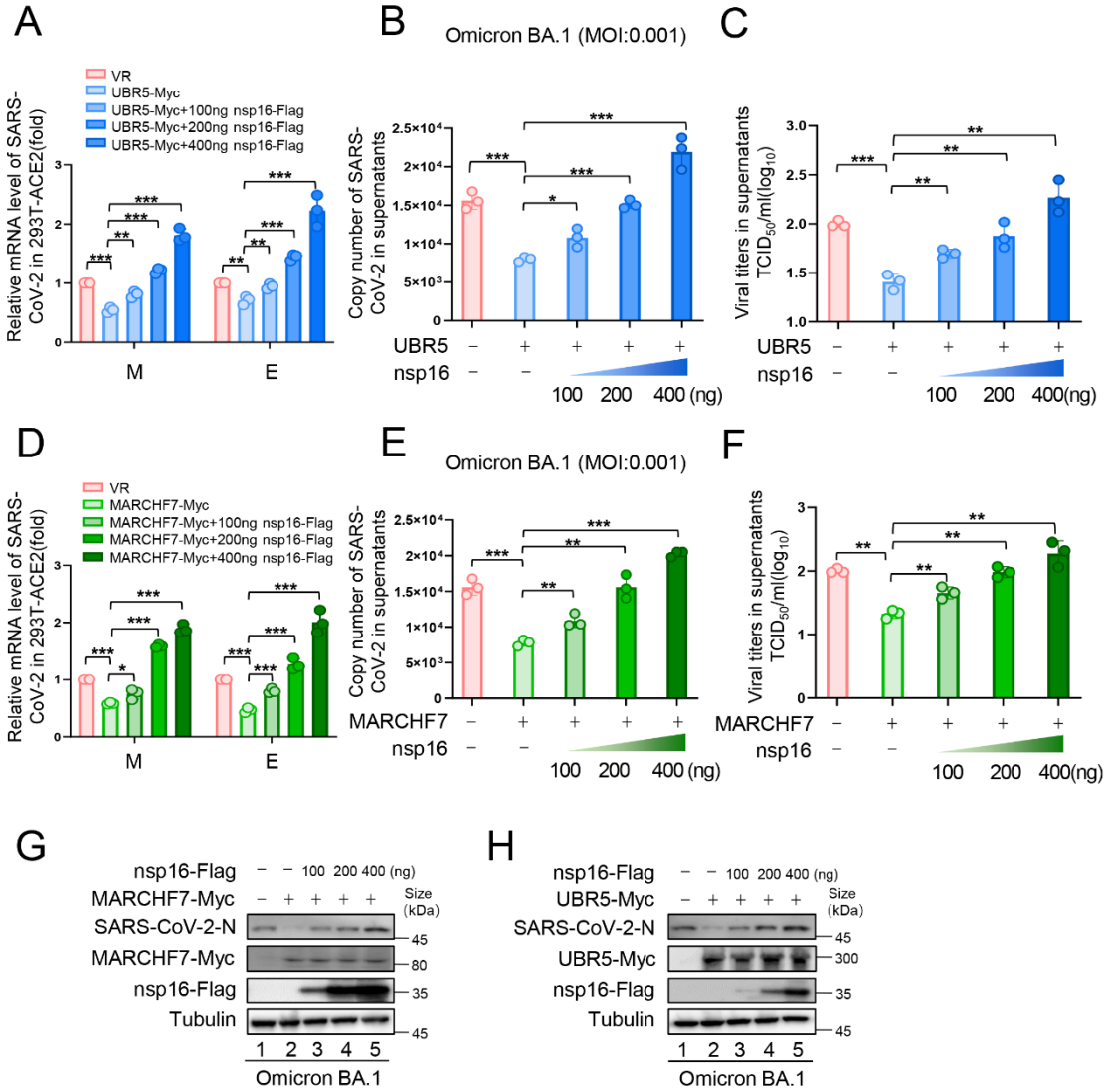

Figure 6 supplement 2

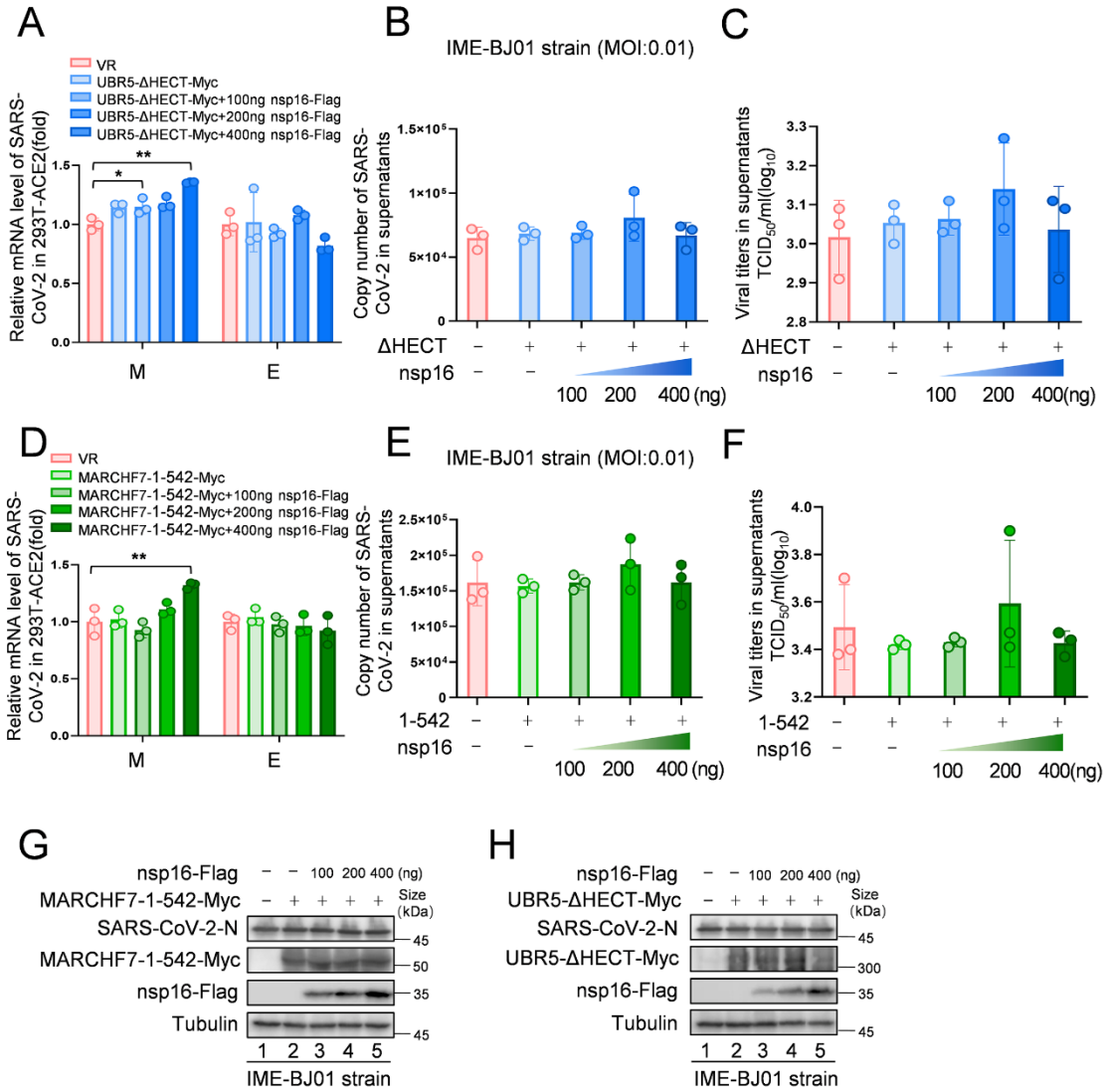

Figure 6 supplement 3

A

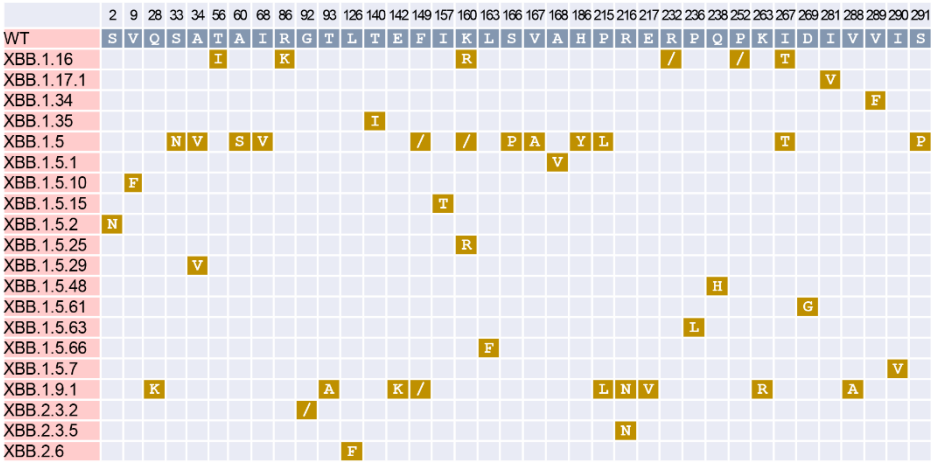

B

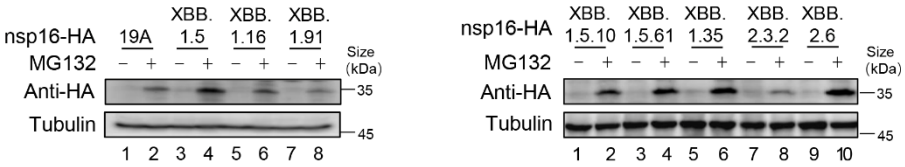

C

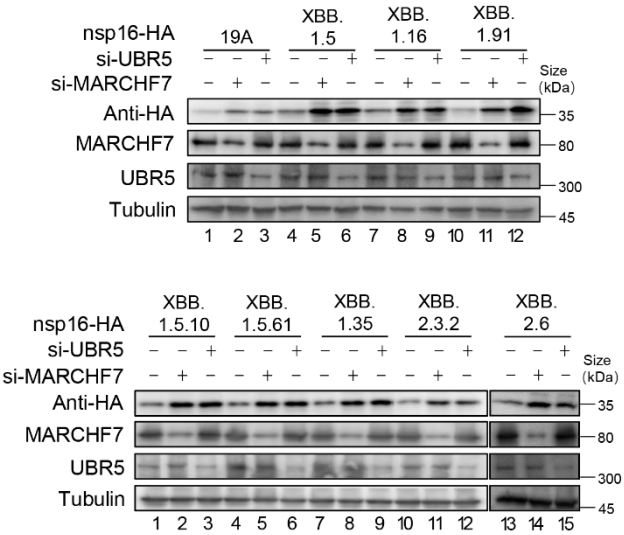

Figure 6 supplement 4

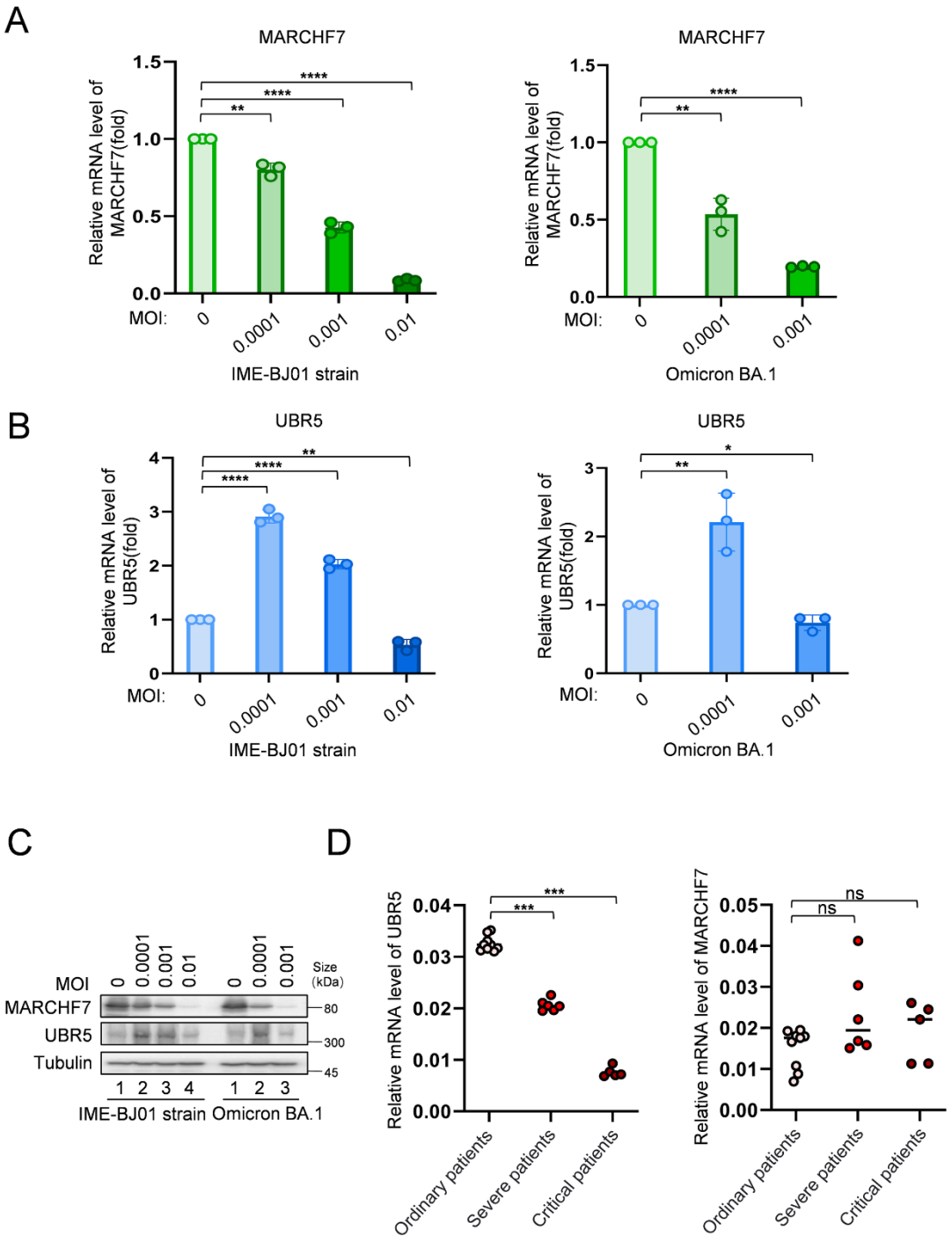

Figure 7

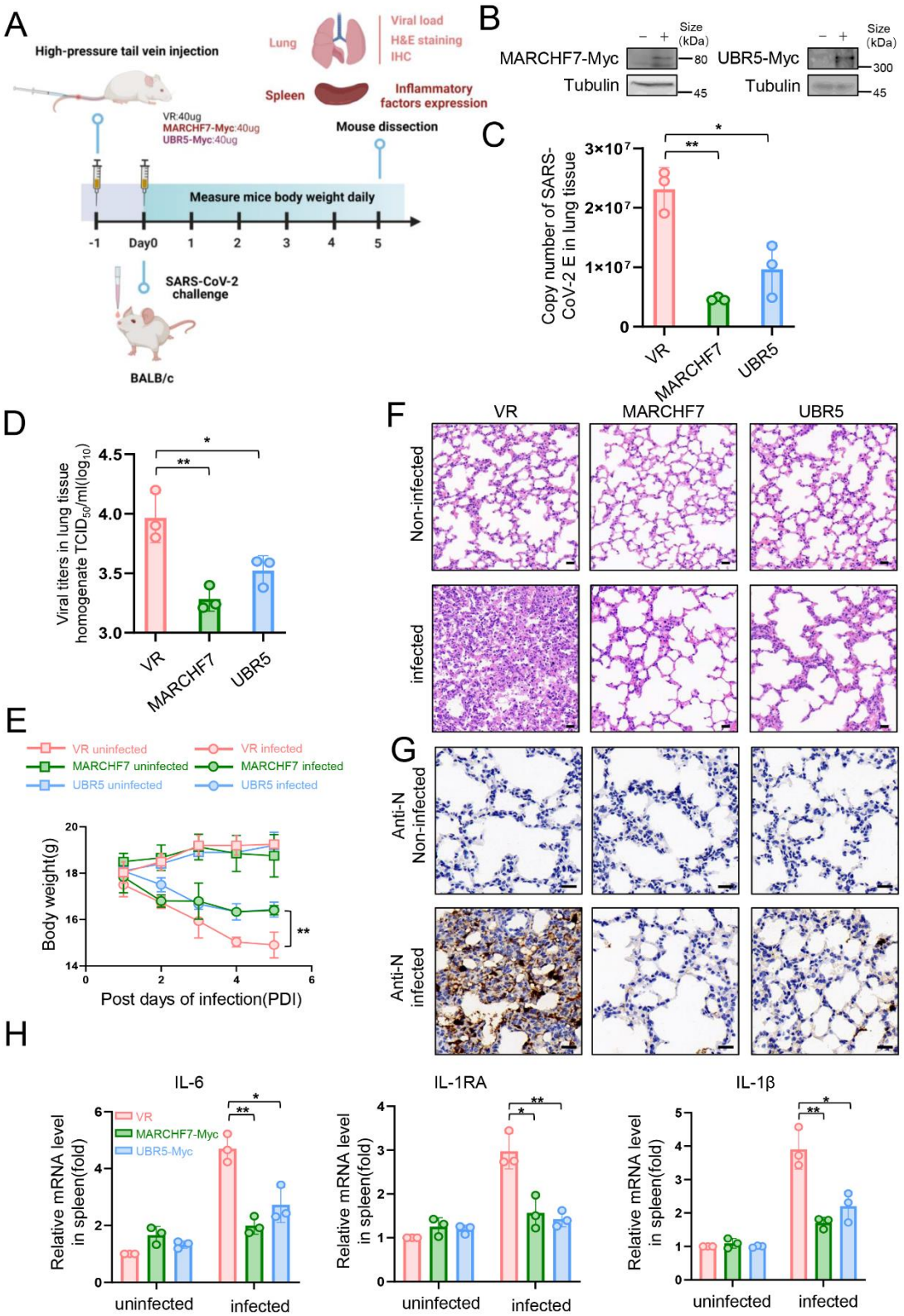
A
High-pressure tail vein injection
Lung
Viral load
H&E staining
IHC
Spleen
Inflammatory factors expression
VR:40ug
MARCHF7-Myc:40ug
UBR5-Myc:40ug
Mouse dissection
Measure mice body weight daily
-1
Day0
1
2
3
4
5
SARS-CoV-2 challenge
BALB/c
B
MARCHF7-Myc
UBR5-Myc
Tubulin
Size (kDa)
80
300
45
C
Copy number of SARS-CoV-2 E in lung tissue
VR
MARCHF7
UBR5
D
Viral titers in lung tissue homogenate TCID50/ml(log10)
E
VR uninfected
MARCHF7 uninfected
UBR5 uninfected
VR infected
MARCHF7 infected
UBR5 infected
Body weight(g)
Post days of infection(PDI)
F
Non-infected
infected
G
Anti-N Non-infected
Anti-N infected
H
IL-6
IL-1RA
IL-1β
VR
MARCHF7-Myc
UBR5-Myc
Relative mRNA level in spleen(fold)
uninfected
infected

Figure 8

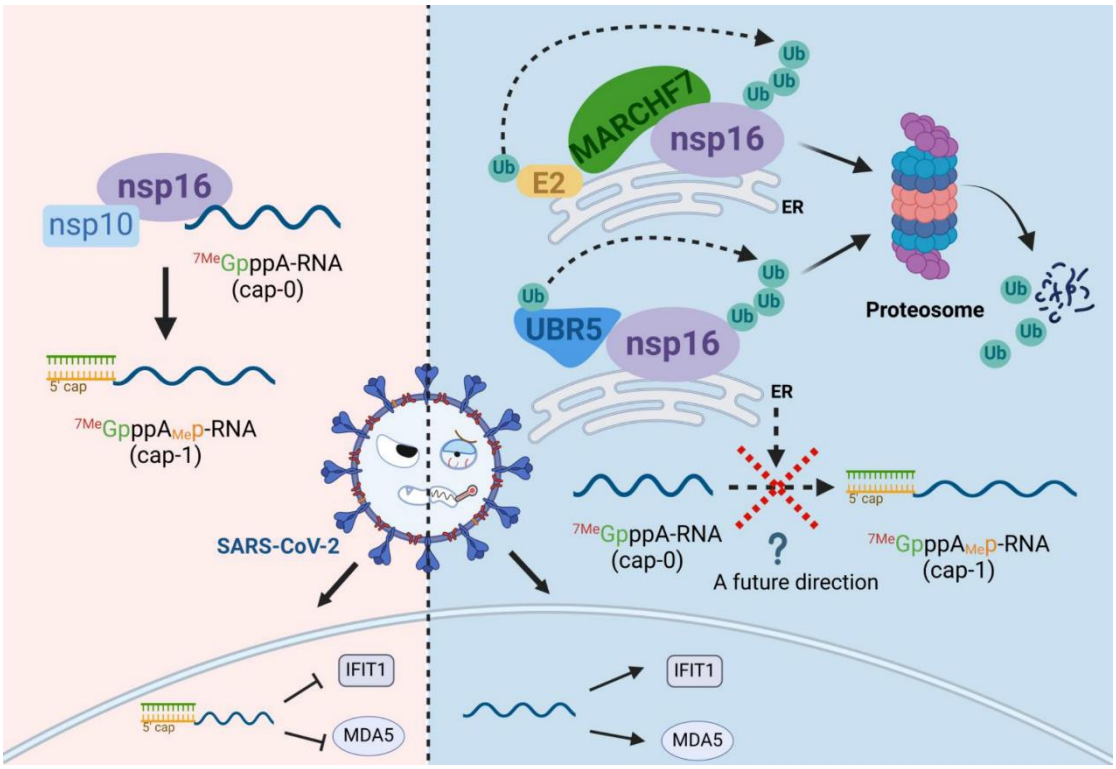
nsp16
nsp10
7MeGpppA-RNA
(cap-0)
5' cap
7MeGpppAMeP-RNA
(cap-1)
SARS-CoV-2
IFIT1
MDA5
5' cap
MARCHF7
nsp16
Ub
E2
ER
UBR5
nsp16
Proteosome
7MeGpppA-RNA
(cap-0)
?
A future direction
7MeGpppAMeP-RNA
(cap-1)
IFIT1
MDA5

eLife Assessment

This important work advances our understanding of how the SARS-CoV-2 Nsp16 protein is regulated by host E3 ligases to promote viral mRNA capping. Support for the overall claims in the revised manuscript is convincing . This work will be of interest to those working in host-viral interactions and the role of the ubiquitin-proteasome system in viral replication.

Public Reviews:

Reviewer #1 (Public review):

In this study, Tiang et al. explore the role of ubiquitination of non-structural protein 16 (nsp16) in the SARS-CoV-2 life cycle. nsp16, in conjunction with nsp10, performs the final step of viral mRNA capping through its 2'-O-methylase activity. This modification allows the virus to evade host immune responses and protects its mRNA from degradation. The authors demonstrate that nsp16 undergoes ubiquitination and subsequent degradation by the host E3 ubiquitin ligases UBR5 and MARCHF7 via the ubiquitin-proteasome system (UPS). Specifically, UBR5 and MARCHF7 mediate nsp16 degradation through K48- and K27-linked ubiquitination, respectively. Notably, degradation of nsp16 by either UBR5 or MARCHF7 operates independently, with both mechanisms effectively inhibiting SARS-CoV-2 replication in vitro and in vivo. Furthermore, UBR5 and MARCHF7 exhibit broad-spectrum antiviral activity by targeting nsp16 variants from various SARS-CoV-2 strains. This research advances our understanding of how nsp16 ubiquitination impacts viral replication and highlights potential targets for developing broadly effective antiviral therapies.

Strengths:

The proposed study is of significant interest to the virology community because it aims to elucidate the biological role of ubiquitination in coronavirus proteins and its impact on the viral life cycle. Understanding these mechanisms will address broadly applicable questions about coronavirus biology and enhance our overall knowledge of ubiquitination's diverse functions in cell biology. Employing in vivo studies is a strength.

Weaknesses:

Minor comments:
Figure 5A- The authors should ensure that the figure is properly labeled to clearly distinguish between the IP (Immunoprecipitation) panel and the input panel.

Reviewer #3 (Public review):

Summary:

The manuscript "SARS-CoV-2 nsp16 is regulated by host E3 ubiquitin ligases, UBR5 and MARCHF7" is an interesting work by Tian et al. describing the degradation/ stability of NSP16 of SARS CoV2 via K48 and K27-linked Ubiquitination and proteasomal degradation. The authors have demonstrated that UBR5 and MARCHF7, an E3 ubiquitin ligase bring about the ubiquitination of NSP16. The concept, and experimental approach to prove the hypothesis looks ok. The in vivo data looks ok with the controls. Overall, the manuscript is good.

Strengths:

The study identified important E3 ligases (MARCHF7 and UBR5) that can ubiquitinate NSP16, an important viral factor.

Comments on revisions:

I had gone through the revised form of the manuscript thoroughly. The authors have addressed all of my concerns. To me, the experimental approach looks convincing that the host E3 ubiquitin ligases (UBR5 and MARCHF7) ubiquitinate NSP16 and mark it for proteasomal degradation via K48- and K27- linkage. The authors have represented the final figure (Fig.8) in a convincing manner, opening a new window to explore the mechanism of capping the vRNA bu NSP16.

Responses：

Manuscript Number: eLife-RP-RA-2024-102277

Title: SARS-CoV-2 nsp16 is regulated by host E3 ubiquitin ligases, UBR5 and MARCHF7

Dear Editor and Reviewers,

We sincerely appreciate the reviewers and editors for recognizing the significance of our experimental findings and for their time and effort during the review process. We are also grateful for the valuable comments, which have helped improve the completeness of our manuscript. Following the reviewers' suggestion—*The authors should ensure that the figure is properly labeled to clearly distinguish between the IP (Immunoprecipitation) panel and the input panel.* —we have carefully corrected the labeling and updated the figure accordingly. Once again, we truly appreciate your meticulous review and constructive feedback.
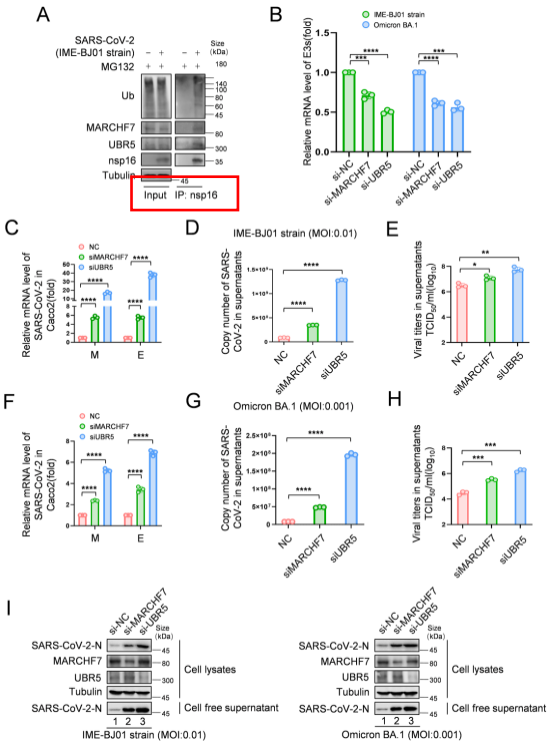
Figure.5